



Chem Soc Rev

**Printing thermoelectric inks toward next-generation energy
and thermal devices**

Journal:	<i>Chemical Society Reviews</i>
Manuscript ID	CS-SYN-05-2021-000490.R2
Article Type:	Review Article
Date Submitted by the Author:	12-Oct-2021
Complete List of Authors:	Zeng, Minxiang; University of Notre Dame, Department of Aerospace and Mechanical Engineering Zavanelli, Duncan; northwestern university, Materials Science and Engineering Chen, Jiahao; University of Notre Dame, Department of Aerospace and Mechanical Engineering Saeidi-Javash, Mortaza; University of Notre Dame, Department of Aerospace and Mechanical Engineering Du, Yipu; University of Notre dame, Department of Aerospace and Mechanical Engineering LeBlanc, Saniya ; George Washington University, Mechanical & Aerospace Engineering Snyder, G.; Northwestern University, Materials Science Zhang, Yanliang; University of Notre dame, Department of Aerospace and Mechanical Engineering

SCHOLARONE™
Manuscripts

ARTICLE

Received 00th January 20xx,
Accepted 00th January 20xx

DOI: 10.1039/x0xx00000x

Printing thermoelectric inks toward next-generation energy and thermal devices

Minxiang Zeng,^{a,*} Duncan Zavanelli,^b Jiahao Chen,^a Mortaza Saeidi-Javash,^a Yipu Du,^a Saniya LeBlanc,^c G Jeffrey Snyder^{b,*} and Yanliang Zhang^{a,*}

The ability of thermoelectric (TE) materials to convert thermal energy to electricity and vice versa highlights them as a promising candidate for sustainable energy applications. Despite considerable increases in the figure of merit zT of thermoelectric materials in the past two decades, there is still a prominent need to develop scalable synthesis and flexible manufacturing processes to convert high-efficiency materials into high-performance devices. Scalable printing techniques provide a versatile solution to not only fabricate both inorganic and organic TE materials with fine control over the compositions and microstructures, but also manufacture thermoelectric devices with optimized geometric and structural designs that lead to improved efficiency and system-level performances. In this review, we aim to provide a comprehensive framework of printing thermoelectric materials and devices by including recent breakthroughs and relevant discussions on TE materials chemistry, ink formulation, flexible or conformable device design, and processing strategies, with an emphasis on additive manufacturing techniques. In addition, we review recent innovations in the flexible, conformal, and stretchable device architectures and highlight state-of-the-art applications of these TE devices in energy harvesting and thermal management. Perspectives of emerging research opportunities and future directions are also discussed. While this review centers on thermoelectrics, the fundamental ink chemistry and printing processes possess the potential for applications to a broad range of energy, thermal and electronic devices.

1. Introduction

The ability of thermoelectric (TE) materials to convert heat into electricity and vice versa has sparked tremendous research interest in the development of high-efficiency thermoelectric materials and devices. It was estimated that ~60% of all fuels used by industry and transportation become waste heat (mostly low-grade heat), which could potentially translate to 15 terawatts of electricity globally.¹ The recovery of thermal energy will not only bring huge energy saving and economic benefits, but also alleviate the heavy reliance on fossil fuels and thus reduce the emission of greenhouse gases. Owing to their versatility and the advantage of adapting to various heat sources, conformal and flexible thermoelectric generators (TEG) are attractive options for energy harvesting to power sensors (e.g., for remote structural health monitoring and commercial plants), biomedical devices, and wearable electronics.² In

addition, TE devices also have broad applications in localized cooling, refrigeration and thermal management. However, conventional TE devices are based on rigid bulk materials, and their cost is not competitive enough compared with state-of-the-art energy conversion technologies. To make TE technology a commercially viable technology, advanced manufacturing strategies are needed to further improve device scalability, reduce materials cost, and improve system-level performances.

Conventionally, various materials fabrication technologies including arc melting, ball milling, and spark plasma sintering techniques have been extensively investigated for TE applications.³⁻⁶ However, these methods typically require expensive facilities and involve energy- and labour-intensive processes, which are not only unsuitable for fast prototyping and low-cost manufacturing, but also pose challenges for producing conformal/flexible TE devices. An alternative method to fabricate conformal/flexible devices is additive manufacturing, such as 2D or 3D printing.⁷ Thus far, a large number of ink-based printing techniques have been developed, including screen printing, inkjet printing, aerosol-jet printing, extrusion printing, roll-to-roll printing, and other additive manufacturing methods.⁸⁻¹² These ink-based printing methods are particularly advantageous for fabricating thin/thick film

^aDepartment of Aerospace and Mechanical Engineering, University of Notre Dame, Notre Dame, IN 46556, USA. Email: mzung2@nd.edu; yzhang45@nd.edu.

^bDepartment of Materials Science & Engineering, Northwestern University, Evanston, IL 60208 USA. Email: jeff.snyder@northwestern.edu.

^cDepartment of Mechanical & Aerospace Engineering, George Washington University, 801 22nd St. NW, Suite 739, Washington, DC 20052, USA.

devices with controlled shape and geometry, while some 3D printing approaches are also used for building bulk TE generators. Thanks to high-resolution printing and good compatibility with a wide range of materials, printing TE materials has led to recent innovations in energy devices, including highly flexible TE components,¹³ stretchable/wearable TEGs,¹⁴ and geometrically versatile TE devices.¹⁵

Despite recent developments in the printing of functional TE devices, a comprehensive understanding of the interplay of materials chemistry, processing strategies, and device designs is missing, particularly at the ink level. In this review, we propose a bottom-up framework to elaborate fundamental correlations between material synthesis, ink formulation, device design, printing processes, and device applications. This review begins with a discussion on thermoelectric device design principles, highlighting the advantages of printing-based methods in achieving high-performance, low-cost, and flexible/conformal devices. The state-of-the-art advances in thermoelectric ink chemistry are sequentially discussed including material synthesis, doping engineering, and ink formulation. Then, various types of printing methods leveraging functional TE inks are introduced, followed by a brief summary of recent developments in conformal/flexible devices. Since TE devices are not limited to energy harvesting applications, we expand our discussion on device applications to other emerging fields, such as thermal management and temperature sensing. In the end, promising directions and research opportunities for printing-related TE technologies are considered together with possible challenges in mass commercialization. This review aims to summarize the emerging materials processing and device manufacturing techniques, elucidate the processing-structure-property relationship of printed materials and systems, and provide an impetus toward fast development of this highly interdisciplinary research field covering both nanoscale building blocks and macroscopic energy devices and systems. In addition, the fundamental ink chemistry and printing processing schemes in this review are highly general and could be applicable to a broad range of technologies far beyond thermoelectrics, such as printed electronics and sensors, printed solid-state batteries, and printed photovoltaics. It should be noted that this review mainly focuses on electronic thermoelectric materials and devices, while thermogalvanic cells and the thermophoresis-based devices are beyond the scope of the review and can be found in other recent reviews.¹⁶

2. Overview

2.1. Thermoelectric figure of merit and device design principles

Thermoelectric devices follow a set of design principles that can be exploited by the adaptability and versatility of ink printing processes. TEGs are typically designed to maximize their power output P , which involves both the device efficiency η and the supplied heat flow Q , where $P = \eta Q$. The efficiency η depends on the temperature differences across the thermoelectric elements such that $\eta = \eta_r (\Delta T_{TE}/T_h)$,

$$P = \eta_r \frac{\Delta T_{TE}}{T_h} Q$$

where η_r is the reduced device efficiency, which is a function of the thermoelectric figure of merit, zT . The material zT is dependent on the Seebeck coefficient and electrical and thermal conductivity as $zT = \sigma S^2 T / \kappa$. Increasing the material zT directly increases efficiency, which in turn increases power output.

$$\eta_r = \frac{\sqrt{1+zT} - 1}{\sqrt{1+zT} + \frac{T_c}{T_h}}$$

Most thermoelectric research focuses on improving material zT because of this relationship. The power factor (PF = σS^2) of TE materials can also be a useful metric when κ is difficult to measure. In addition, while the importance of zT is well understood, there are other parameters that need to be optimized for TEG design. For example, it is imperative not to neglect the need for heat flow, Q , in calculating the power output. Unfortunately, many choices in device design, such as TE element length, change these terms in opposite directions. The heat flow Q is limited by the capability of the TE device to exchange heat with its surroundings both on the hot and the cold side of the device. The heat transfer capability of the heat exchangers can be expressed as the inverse of the thermal impedance of the heat exchangers, $1/\theta_{HX}$, which ultimately determines the heat flow Q in the TE device based on a given external temperature gradient.

In addition to the heat exchanger, the thermal impedance of the thermoelectric device θ_{TE} must also be considered. Too small of a θ_{TE} would lead to a low power output because of a small temperature drop across the thermoelectric $\Delta T_{TE} = Q\theta_{TE}$. However, an extremely high θ_{TE} would also lead to low power output. Under a constant temperature boundary condition, a large θ_{TE} would increase ΔT_{TE} , resulting in a decrease in the temperature drop across the heat exchangers ΔT_{HX} and a decreased Q . As a result of the above trade-off, the TEG power output is maximized when the internal and external thermal impedances are identical $\theta_{TE} = \theta_{HX}$ in a situation similar to impedance matching in traditional electronics for components placed in series. This condition gives a function for the device power that is dependent only on materials properties and the temperatures of supplied heat (heat source and heat sink):¹⁷

$$P = \eta_r \frac{\Delta T_{supply}^2}{T_h} \times \frac{\theta_{TE}}{(\theta_{HX} + \theta_{TE})^2}$$

The impedance of heat exchangers can be calculated by $\theta_{HX} = 1/h_{HX}A_{HX}$, where h_{HX} and A_{HX} are the effective heat transfer coefficient and the area of the heat exchanger. The impedance of the TE device can be calculated by $\theta_{TE} = l/\kappa_{eff}A_{HX}f$, where l and κ_{eff} are the length and effective thermal conductivity¹⁸ of the TE elements, and f is the filling factor of the TE elements, $f = A_{TE}/A_{HX}$.

The impedance matching requirement thus gives a relation for the device geometries that maximize the power density (power output per area) of a TEG²:

$$l = \frac{f\kappa_{eff}}{h_{HX}}$$

From this relationship, impedance matching can be achieved by controlling the length of thermoelectric elements and the filling fraction of TE elements in the device. Often the

optimum l is greater than typical thicknesses of films fabricated by traditional thin film deposition methods,¹⁹ making printing technologies ideal to achieve a much greater range of TE element thickness from micrometres to millimetres. The printed thermoelectric materials typically have lower κ_{eff} due to porosity and other defects, allowing shorter lengths and larger filling factor of TE elements. Moreover, additive manufacturing methods have led to the fabrication of advanced heat exchangers with significantly improved h_{hx} compared with traditional heat exchangers, further reducing the optimal length l of TE elements and enabling relatively thin and flexible TEGs.

This analysis of TEG power output dictates how thermoelectric materials should be designed and evaluated. The power output of the system under thermal impedance matching conditions is a function of efficiency and thus material zT . As a result, material zT should be optimized rather than material power factor.²⁰ In addition, the doping level needed to optimize zT is different than that needed to optimize the power factor of a thermoelectric material.²¹ However, measuring the thermal conductivity of printed materials can be very difficult especially for printed thin films and thus power factor is often the only metric reported. It is thus important to recognize that this metric will not directly correlate to device efficiency and power output and is an imperfect comparison between materials. In addition, the impedance matching condition means the output power is proportional to the device area as well as ΔT^2 . Any comparison of TEGs must therefore include both the ΔT and area to be able to compare power output or power density.

The device figure of merit ZT can be reported for a complete thermoelectric device. Device ZT can be approximated as

$$ZT = \frac{S^2}{\kappa R} T$$

where S is the overall device Seebeck coefficient, κ and R are the thermal conductance and electrical resistance of the device, and T is the average device operating temperature. Optimizing this factor will satisfy the conditions for optimal power and thus is the most useful metric when comparing TEGs.

2.2. Printing processes to enable high-performance and low-cost device manufacturing

The use of printing originates from ancient China where moveable woodblocks were used for letter reproduction. Nowadays, owing to the ability to efficiently convert materials into devices, printing has been considered as one of the most versatile approaches for rapid prototyping and advanced manufacturing. A wide range of materials, including conductors, semiconductors, and dielectrics, have been leveraged for printing devices for a variety of applications.²²⁻²⁸ Based on the processing conditions, printing techniques can be mainly categorised into two types: mask-based patterning and maskless patterning. The typical mask-based printing strategies include screen printing, roll-to-roll printing, and spray printing, while extrusion printing, inkjet printing, and aerosol jet printing are examples of maskless approaches. Mask-based printing involves a pre-designed template that selectively allows ink to deposit on substrates. By contrast, maskless printing methods rely on nozzle dispensing or selective sintering/curing to

convert starting ink materials into pre-defined 2D/3D patterns. Here we highlight several major advantages of printing technologies to enable high performance, low-cost, and flexible/conformal thermoelectric materials and devices.

Printing methods provide a highly scalable and efficient manufacturing process to directly transform thermoelectric inks into microscale/macroscale devices. The printing process can eliminate the labor-intensive processes and material waste in conventional TE device fabrication, such as hot pressing of TE disks, dicing TE elements, and assembling and joining TE elements with metal electrodes. Printed thermoelectric devices can realize optimized TE element thickness and geometry for producing maximum power density with minimum materials consumption, which significantly reduces device cost. Joining thermoelectric materials to metal contacts with low contact resistivity and high bonding strength is one of the most critical processes in TE device fabrication. Multiple metallic layers (diffusion barriers, solder, electrodes, etc.) can be readily printed on the TE materials to obtain stable electrical contacts with low resistances. Printing methods are highly scalable to fabricate both microscale devices for energy harvesting/thermal management and macroscale devices for industrial waste heat recovery applications.

The recent development of multi-material printing methods enables the manufacturing of nanocomposite materials of various compositions and sophisticated structures in a high-throughput manner. The versatility of additive manufacturing processes allows synergistic integration of virtually any materials (e.g. organic and inorganic nanocrystals) with highly complementary thermoelectric and mechanical properties. These nanocomposites may or may not have increased zT over the single constituent but will likely have improved mechanical properties required for making robust devices. In addition, printing methods facilitate the integration of multiple TE materials with segmented structures or gradient compositions/doping such that the zT of each constituent material peaks at the corresponding operating temperature range. In this way, an increased average zT can be realized in the graded TE elements for use in large temperature differences.^{29, 30}

Printing methods can be applied to integrate TE materials with flexible substrates or support structures to produce highly flexible devices. The flexible TE devices can greatly facilitate integration with various heat sources on curved surfaces, such as human body integration for powering wearable devices, and integration with industrial systems to power sensors and industrial internet of things. The fabrication of flexible TE devices can leverage the rapid technology advancement of printed electronics and roll-to-roll printing, which can make thermoelectrics a cost-effective and commercially viable technology.

The 3D conformal printing methods (e.g. aerosol jet printing) allow direct printing of TE devices onto heat-source components or cooling surfaces for intimate integration with end-user systems. Furthermore, low-thermal-resistance and compact heat exchangers are critical to achieving high heat flow and high power density. Advanced printing methods can

manufacture compact thermoelectric systems with fully integrated heat exchangers and greatly reduce the thermal resistances of various components and their interfaces, leading to improved system-level performances.

Despite vast variations among different printing technologies, a typical printing process involves device pattern design, ink formulation, printing, and post-printing processing. In order to realize high-performance and low-cost printed

devices, a holistic approach needs to be taken to judiciously design and optimize all these critical processing steps. This article aims to systematically review material synthesis, ink formulation, device design, printing and post-printing processing strategies, and device applications as well as to elucidate the processing-structure-property relationship of printed thermoelectric systems.

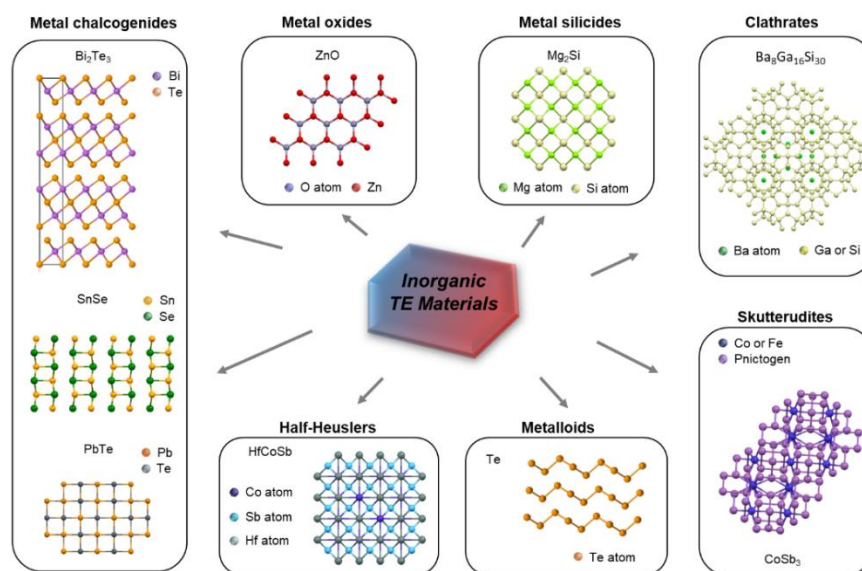


Figure 1. Examples of inorganic thermoelectric materials.

3. Thermoelectric inks

3.1. Synthesis of thermoelectric materials

3.1.1 Inorganic materials

Since the discovery of Bi_2Te_3 in the 1950s, a great number of synthetic strategies have been explored to prepare thermoelectric materials. Depending on the operation temperature, there have been a great number of thermoelectric materials developed for energy conversion applications (Figure 1). In the 300–450 K range, Bi_2Te_3 , Sb_2Te_3 , and Ag_2Se have been extensively investigated.³¹ In the 450–900 K range, PbTe , PbSe , half-Heuslers and skutterudites are the popular choices.³² In the high temperature range ($T > 750$ K), SnSe and SiGe show superior performance.³³ These thermoelectric materials can be readily fabricated using an “alloying” approach where precursor elements are weighed, mixed, and processed at an elevated temperature. The advantages of this method include the accurate control of material chemical composition and minimization of possible contamination, though solid-state syntheses remain challenging to scale up, and they are not well controllable in terms of morphology and microstructures of TE materials.³⁴ More importantly, the TE particles synthesized by solid-state syntheses lack ligand/surfactant on the surface and tend to aggregate severely in the ink phase, which makes them not compatible with some printing approaches (e.g., inkjet printing).^{7, 35, 36} Alternatively, solution-based wet-chemistry methods have emerged as a potent synthetic approach for

inorganic TE materials as they enable facile control of particle size, electronic structures, and surface chemistry.^{34, 37} Currently, solution-based synthetic routes have been explored for synthesizing metals, chalcogens/chalcogenides, and oxides.³⁸ In addition, the wet-chemistry production of antimonides and Si–Ge has been studied, though techniques that enable scalable fabrication of numerous potential thermoelectric compounds need further exploration.^{34, 39}

In a typical solution-based synthesis route, proper selection of starting materials, such as precursors, redox agents, surfactants and solvents, is crucial for synthesizing high-quality nanoparticles. To maximize the reaction yield and avoid side reactions, the reaction temperature profile needs to be judiciously designed. For example, the reducing agent hydrazine should be added under 120 °C (before further increasing reaction temperature) due to its low boiling point (~114 °C).⁴⁰ After the reaction is completed, careful purification that effectively removes byproducts/unreacted starting materials is essential as impurities can significantly affect the thermoelectric properties of TE materials. Taking metal tellurides (e.g., Bi_2Te_3 ⁴¹) as examples, Te precursors, bases, surfactants, precursors of the metal cations (e.g., $\text{Bi}(\text{NO}_3)_3 \cdot 5\text{H}_2\text{O}$) are added to the high boiling point solvents (e.g., ethylene glycol), followed by dissolution with the assistance of either sonication or heating. After the addition of reducing agents, the dispersion is heated to an elevated temperature. For reducing agents, hydroxylamine (for

Bi_2Te_3 and Bi_2Se_3 , trioctylphosphine (for Bi_2Te_3), and NaBH_4 (for SnSe) are commonly employed for synthesizing nanostructured metal chalcogenides.³⁴ For cations that can be readily reducible (such as Ag_2Te ⁴² or Cu_{2-x}Te ⁴³), the use of aforementioned strong reducing agents can be avoided because solvents like ethylene glycol can reduce the cations into metals. In addition, under high reaction temperature, thermoelectric particles such as Bi_2Te_3 ⁴⁴ or PbTe ⁴⁵ have been fabricated simply using ethylene glycol without any additional strong reducing agent.

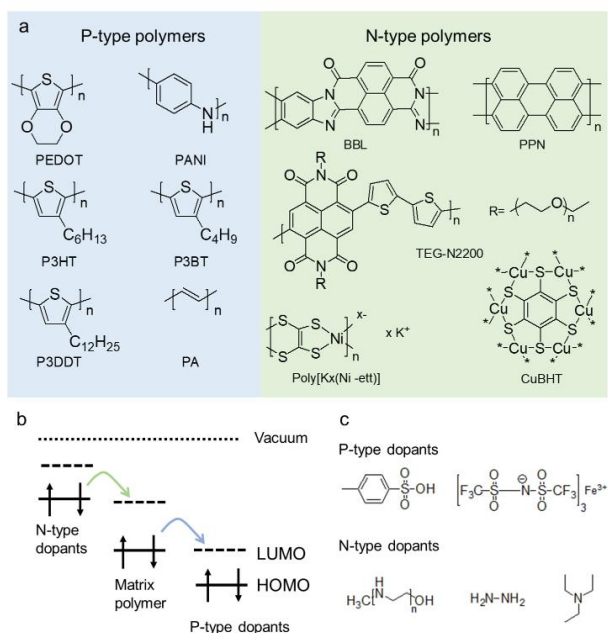
3.1.2 Organic materials

Conductive polymers, such as polypyrrole (PPy), poly(3-hexylthiophene-2,5-diyl) (P3HT), polyaniline (PANI) and poly(3,4-ethylenedioxythiophene) (PEDOT), have been widely studied for advanced energy and device applications including biosensors and electrochemical capacitors.^{46,47} **Figure 2a** shows several examples of conductive polymers that have been also studied as TE materials. Either wet-chemistry polymerization or electrochemical polymerization can be used to synthesize the polymers, with or without catalysts.⁴⁸⁻⁵⁰ For example, the synthesis of thermoelectric PEDOT can be achieved by polymerizing 3,4-ethylenedioxythiophene in presence of iron(III) trifluoromethanesulfonate ($\text{Fe}(\text{OTf})_3$), where the iron(III) was used as both initiator and dopant.⁵¹ The electronic properties, such as conductivity, are highly dependent on the doping of the polymers, as doping can significantly influence the carrier concentration and bandgap of the conductive polymers.⁵² Typically, n-type dopants provide electrons to the lowest unoccupied molecular orbital (LUMO) of matrix polymers (**Figure 2b**), whereas in p-type doping the electron moves from the highest occupied molecular orbital (HOMO) of the polymers to the p-type dopant species and creates a hole in the polymer backbone.⁵³

Figure 2. a) Examples of p-type and n-type thermoelectric polymers and their doping mechanism. b) Doping mechanism to tailor the transport properties of TE polymers. c) Examples of p-type and n-type dopants.

For thermoelectric applications, these conductive polymers are usually highly doped, chemically or electrochemically. Several chemical dopants have been demonstrated, as shown in **Figure 2c**. Redox reactions allow electrons to transfer between polymer backbones and dopant molecules (in chemical doping) or electrodes (in electrochemical doping). Acid/base doping involves proton transfer processes, where H^+ is bonded on polymer backbones without changing oxidation numbers. For polymer synthesis or preparation, polymerization conditions can be harnessed to tune nanoscale or microscale morphologies of the materials. Yu and co-workers reported a supramolecular method to synthesize structured polypyrrole, where various molecules were used as crosslinkers to form polymer nanowires.⁵⁴ They also found that the morphology and structural parameters of the polypyrrole can be tuned by using different initiators and dopant molecules and varying their concentrations in the synthesis. In TE materials, arguably the most important two properties, electrical conductivity and Seebeck coefficient, are mostly related to carrier concentration (and often mobility⁵⁵ as well). Doping in the conjugated polymers introduces charge carriers and renders them conductive. The generation of charge carriers in conductive polymers is complicated, but it is generally considered the creation of polarons and bipolarons in the polymer chain.^{56,57} In some cases, such as polyacetylene, the solitons created by doping form a soliton band and result in metallic conductivity.⁵⁶ Polarons and bipolarons can be detected with electron spin resonance (ESR) techniques, ultraviolet-visible and near-infrared (UV-vis-NIR) spectroscopy, and Raman spectroscopy. Similar to all organic electronic materials, the crystallinity and morphologies of TE polymers determine the charge transport mechanisms. However, doping levels, conformation, and the stacking manners of molecules can affect the (bi)polarons, and hence the charge carrier transport behaviour. To achieve desirable thermoelectric properties, dopant concentrations, chemical structures of the molecules, counterions effect, and the resultant molecular arrangement should be taken into account in designing the materials.

In addition to electrical conductivity, thermal conductivity or mobility of heat in conductive polymers also needs to be engineered for TE applications. Similar to inorganic materials, heat is transported in conductive polymers by phonons and charge carriers. However, the Wiedemann-Franz law in inorganic metals and semiconductors is often invalid in conjugated polymers because of their stronger charge-lattice coupling.^{58,59} It is widely acknowledged that the charges in conducting polymers could induce lattice deformation and thus could be localized. Charge transport is therefore significantly restricted by such localization of the charges in conductive polymers, blocking the thermal transport.⁶⁰ Thus it is generally understood that thermal transport in conductive polymers can be dominated by phonons. However, a linear correlation



between electronic thermal conductivity (κ_e) or phonons (κ_p) with thermal conductivity, as $\kappa = \kappa_e + \kappa_p$, is oversimplified due to the strong and complicated interactions between electrons and lattice vibrations in conducting polymers. Wang et al. reported that not only the polaron (charge and phonon) but also the interaction energy between charges and lattice vibrations make significant contribution to the thermal transport in conductive polymers such as poly(3-hexylthiophene-2,5-diyl) (P3HT) and poly(3,4-ethylenedioxythiophene)-poly(styrenesulfonate) (PEDOT:PSS).⁶¹

Conductive polymers show promising TE properties; however, the dependence of thermal conductivity on synthesis conditions and molecular structures has not been sufficiently investigated.⁴⁸ Historically, the challenge of reliably measuring thermal conductivity along the same direction as the electrical conductivity of polymer films makes reporting power factor more relevant for conductive polymers. More recently, it has been reported that the crystallinity of the polymer materials, alignment of polymer chains, and domain interfaces or grain boundaries may affect the thermal conductivity of polymer films or fibers.⁶²⁻⁶⁴ This also brings the challenge that the current minimum thermal conductivity model can only explain the thermal conductivity of amorphous polymers. Understanding the heat transport in conductive polymers is yet still an ongoing effort.⁶⁵

Low thermal conductivity and mechanical compliance of conductive polymers make them good candidates for thermoelectric units in wearable devices or flexible TEG. The overall thermoelectric performance of such organic TEG, however, still needs to be improved for practical use. To develop organic thermoelectric devices with satisfactory overall zT values, further development is needed to understand the conductivity and Seebeck coefficient of crystalline conductive polymers.

In addition to the thermoelectric effect based on electronic transport, ion-based thermoelectric phenomena have also been reported,^{66,67} typically including thermogalvanic effect (induced by the temperature-dependent entropy changes that involve electrochemical reactions) and Soret effect (i.e., the thermodiffusion of cations and anions without electrochemical reactions). A number of ion-based thermoelectric systems including ferri/ferrocyanide ($[\text{Fe}(\text{CN})_6]^{4-}/[\text{Fe}(\text{CN})_6]^{3-}$),⁶⁸ iron sulphate,⁶⁹ and copper/copper hexacyanoferrate⁷⁰ have shown encouraging potential for harvesting low-grade thermal energy. Due to very limited number of reports on printing ionic thermoelectrics, this review mainly focuses on electronic-based thermoelectric materials and devices. A comprehensive overview of ionic thermoelectric materials and devices can be found in other recent reviews.^{71,72}

3.2. Ink formulation

The recent advancements of solution-based manufacturing methodologies have sparked tremendous research interests in developing functional inks of energy materials, leading to a fascinating variety of printed devices including sensors, supercapacitors, lithium-ion batteries, and solar cells.⁷ In

formulating printable TE inks, the solvent selection is important to the colloidal stability of TE materials. Dispersing thermoelectric materials in solvents requires a suitable solvent that matches the materials or their surface ligands. In addition, the solvent viscosity, surface tension, and Hansen solubility parameters should be considered carefully to disperse nanomaterials in inks.^{73,74} For example, Hansen distance (Ra , also referred as Hansen solubility parameter) is as follows:

$$Ra = \sqrt{(\delta_{D,A} - \delta_{D,B})^2 + (\delta_{P,A} - \delta_{P,B})^2 + (\delta_{H,A} - \delta_{H,B})^2}$$

Where δ_D is the energy from dispersion forces of A and B, δ_P is the energy from dipolar interaction, and δ_H is the energy from hydrogen bonding.

The smaller Ra is, the more likely the two molecules or compounds are to dissolve. As Ra is not readily available for many TE materials, a quick estimation can be made using the polarity of the solvent, as shown in **Figure 3a**. The volatility of solvents can also play an important role in the printing process. For instance, screen-printing techniques use solvents that are less volatile (e.g., terpineol) to avoid possible clogging of the screen mesh related to rapid drying, while highly volatile solvents (e.g., ethanol) are needed for high-speed roll-to-roll printing. For certain ink materials, mixed solvents can further improve the dispersity and ink rheology by tuning the boiling point, surface tension and solubility parameters.^{75,76} To date, most high-quality nanoparticles have been obtained and dispersed using organic solvents, while environmentally friendly solvents such as water provide a cost-effective alternative which would be highly valuable for scalable manufacturing processes.⁷⁷ To use water as a solvent, serious shortcomings such as the oxidative and hydrolyzing abilities of water need to be overcome, and the stability of the thermoelectric material families (e.g. half-Heuslers) must be improved by introducing O_2 scavengers or surface passivation.

For TE polymers, significant effort has been made to improve the solubility/dispersity. Historically, the first generation of conjugated polymers are neither soluble nor fusible due to the strong intermolecular interactions without side substitutes.⁴⁸ One way to improve the polymer solubility is to polymerize monomers with longer side substitutes, resulting in the second development of conjugated polymers. In fact, the improved solubility facilitates the processing of TE polymers as well as the synthesis of polymers with larger molecular weights. Another method is to introduce external species that can facilitate emulsion polymerizations, such as PEDOT:PSS and PANI:camphorsulfonic acid (CSA). Nowadays, PEDOT:PSS of various qualities is commercially available in the form of dispersion in water.

Another factor in the colloidal stability of TE inks is the surface ligands/surfactants used.⁷⁸ For nonpolar solvents, steric repulsion plays a major role in colloidal stability; surface ligands with solvophilic groups (e.g., long-chain alkyl groups) are often required. For polar solvents such as water, colloidal particles can be stabilized electrostatically and/or sterically.⁷⁹⁻⁸⁸ As shown in **Figure 3b**, DLVO theory (named after Boris Derjaguin and Lev Landau, Evert Verwey and Theodoor Overbeek) describes the interaction between charged surfaces in a liquid

medium, quantifying the effects of the van der Waals attraction and the electrostatic repulsion from the double layer of counterions.^{89, 90} Several examples of surfactants can be found in **Figure 3c**. Owing to the steric repulsion or/and electrostatic repulsion, the addition of surfactants can significantly improve the colloidal stability of inks (**Figure 3d**) and allow higher concentrations of TE materials for printing applications. In addition, some studies indicate that surfactants can improve film adhesion via an ink aging process.⁹¹ However, the residue of organic surfactants can negatively affect the thermoelectric properties of the final material, and thus additional thermal processing or purification step is often required to remove these surfactants.⁷

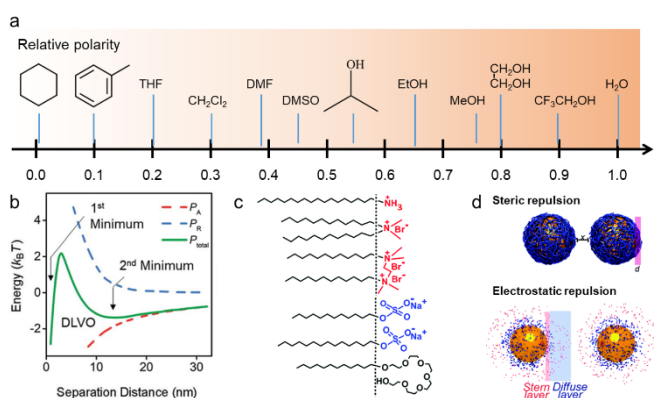


Figure 3. Solvents and surfactant chemistry of ink formulation. (a) Various types of solvents and their relative polarity to water. (b) DLVO profile of a colloidal suspension with the van der Waals and double layer contributions.⁷ (c) Examples of cationic (red), anionic (blue), and nonionic surfactants (black).⁹² (d) Schematic illustration of steric and electrostatic repulsion.⁹³ b-d) adapted from ref. 7, 92, 93 with permission from RSC.

image of a Cu₂Se from Zintl ions, showing a mirror-like reflection.⁹⁴ (d) PbTe NCs and Bi₂S₃ nanorods capped with the organic ligands and a solution of Sb₂Te₃-MCCs (molecular metal chalcogenide complex).⁹⁵ (e) Drop-cast thin film of PbTe NCs capped with Sb₂Te₃-MCCs, spray-coated (Bi,Sb)₂Te₃ thin film with inorganic ligands.⁹⁵ b) Adapted from ref. 38 with permission from RSC. c) Adapted from ref. 94 with permission from Wiley-VCH. d-e) Adapted from ref. 95 with permission from ACS.

As the surface of nanomaterials dominates many physical and chemical processes,⁷⁸ the surface ligand is an important component in ink formulation. Typically, surface ligands can be classified into different types, including X-type, L-type, and Z-type ligands (**Figure 4a**).^{78, 96} X-type ligands are molecules that form a two-electron covalent bond and coordinate with non-neutral cationic sites, such as carboxylates (RCOO⁻) and thiolates (RS⁻). L-type ligands (like phosphines (R₃P)) are neutral two-electron donors with a lone electron pair that coordinates with surface sites, while Z-type ligands (including Pb(OOCR)₂) bind as two-electron acceptors on the particle surface. The type of ligand may also depend on the surface chemistry and reaction sites that it binds with. For example, oleic acid can be used as a bidentate Z-type ligand or as X-type oleate ions depending on the particle surface chemistry.⁹⁶

To further tune surface chemistry and nanomaterials properties, ligand exchange/removal are popular strategies for band engineering, stoichiometry control, and extrinsic doping (**Figure 4b**).³⁸ In addition to conventional organic ligands, inorganic ligands including metal–chalcogenide complexes (MCCs) have been recently demonstrated to enable nanomaterials with relatively high charge carrier mobilities.⁹⁷ In particular, metal chalcogenide complexes not only provide colloidal stability to nanoparticles, but also can be converted into thermoelectric materials by either thermal annealing or laser treatment. For example, Cu₂Se can be generated from Zintl ions, resulting in a mirror-like reflection from the thin film (**Figure 4c**).⁹⁴ PbTe NCs and Bi₂S₃ nanorods can be stabilized using molecular metal chalcogenide complexes (Sb₂Te₃-MCCs, **Figure 4d-f**).⁹⁵ After thermal annealing, Sb₂Te₃-MCCs transformed into Sb₂Te₃ and Te, which facilitate the formation of TE nanocomposites with controlled grain size. In addition to solvents, surfactants, and ligands, various types of polymers have been used as additives in ink formulation (such as polyvinylpyrrolidone).^{98, 99} Some functional polymers can improve ink rheological properties, while others can serve as a colloidal stabilizer and prevent particle aggregation.¹⁰⁰ Ink binders are used to connect nanoparticles to each other and thus form a more robust structure after printing. Several thermoelectric ink formulations consisting of TE materials, solvents, ligands, surfactants, binders, and other additives are shown in **Table 1**.

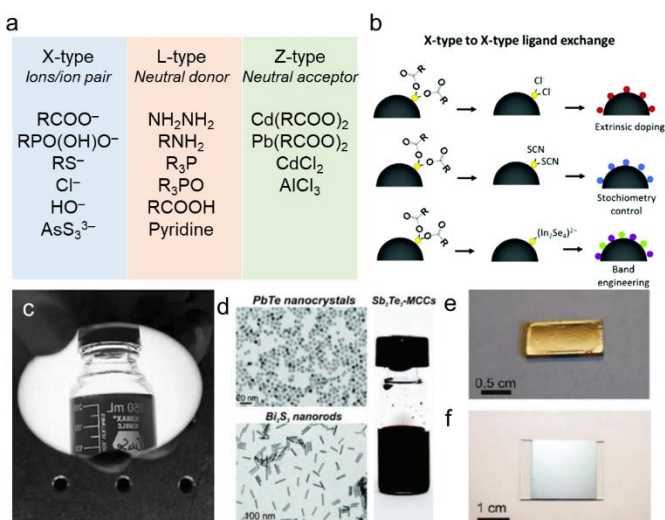


Figure 4. Ligand chemistry and thermoelectric metal chalcogenide ligands. (a) Examples of common surface ligands. (b) Schematic of ligand exchange processes.³⁸ (c) Photographic

Table 1: Examples of thermoelectric ink formulations and printing approaches. *The abbreviations of chemicals are EG: ethylene glycol, HA: hexylammonium chloride, NMF: N-Methylformamide, CNT: carbon nanotube, Gr: graphene. ** The 1-cyanoethyl-2-ethyl-4-methylimidazole was used as a cure accelerator in epoxy systems.

TE materials	Solvent	Ligands/Binders/Additives	Printing methods
$\text{Bi}_{0.4}\text{Sb}_{1.6}\text{Te}_3$	α -Terpineol	Disperbyk-110	Screen printing ¹⁰¹
$\text{Bi}_2\text{Te}_{2.8}\text{Se}_{0.2}$	α -Terpineol	Disperbyk-110/glass frits	Screen printing ¹⁰²
$\text{Bi}_2\text{Te}_{2.7}\text{Se}_{0.3}$	EG/glycerol/ethanol	PVP	Aerosol jet printing ¹⁰³
Sb_2Te_3 -Te	EG/glycerol/ethanol	PVP	Aerosol jet printing ¹⁰⁴
PEDOT:PSS-CNT	Water	SDS/PVP	Aerosol jet printing ¹⁰⁵
V_2O_5 /PEDOT	Water	-	Ink jet printing ¹⁰⁶
Poly[$\text{K}_x(\text{Ni-ett})$] /PVDF	DMSO	-	Ink jet printing ¹⁰⁷
Bi_2Te_3 NW	Water	PVP	Ink jet printing ¹³
$\text{TiS}_2(\text{HA})_x$	NMF	HA	Ink jet printing ¹⁰⁸
$\text{Bi}_2\text{Te}_3/\text{Se}/\text{epoxy}$	Butyl glycidyl ether	1-cyanoethyl-2-ethyl-4-methylimidazole**	Dispenser printing ¹⁰⁹
Te-PEDOT:PSS	Water	-	Dispenser printing ¹¹⁰
$\text{Bi}_{0.5}\text{Sb}_{1.5}\text{Te}_3$	Glycerol	Sb_2Te_4 MCCs	Dispenser printing ¹¹¹
CNT/P3HT	Chloroform	P3HT	Spray printing ¹¹²
N-doped Gr	EG	-	Roll-to-roll printing ¹¹³
PEDOT: PSS	Water	DMSO	Roll-to-roll printing ¹¹³

The ink rheology such as viscosity plays a significant role in the printing consistency and performance. Ink viscosity defines the resistance to flow at a given shear rate.¹¹⁴ Typically, screen printing requires inks with high viscosity, while low-viscosity ink is preferred for inkjet printing. It is worth mentioning that some nanoparticle inks exhibit unique behaviour under shear force,¹¹⁵⁻¹²⁰ such as reduced viscosity at a high shear rate (*i.e.*, shear-thinning behaviour). Kim et al. observed the shear-thinning phenomena for Bi_2Te_3 -based ink.¹¹¹ The authors attribute it to the collapse of the colloidal structure under shear stress. The shear-thinning dispersions allow the ink to flow with less increase in resistance force at a higher shear rate, which facilitates nanoparticle homogenization and ink processing during printing.

4. Ink printing and processing

With the ability of directly transforming thermoelectric inks into TE devices with predesigned patterns and shapes,^{12, 121} a number of printing techniques (such as screen printing, inkjet printing, aerosol-jet printing, etc.) have been investigated extensively, and a wide range of TE materials including inorganic nanoparticles (e.g., Bi_2Te_3 , Sb_2Te_3 , SnSe , $\text{Ca}_3\text{Co}_4\text{O}_9$) and organic polymers (e.g., PEDOT, PPy, PANI) have been successfully integrated in printing processes.^{103, 122-125} Here we review the most applicable printing methods to manufacture TE devices.

4.1. Screen printing

The screen-printing technique is one of the most studied scalable and low-cost printing methods for processing thermoelectric materials as it can tolerate the high viscosity of concentrated TE inks. As a template-based process, screen printing relies on the precise transfer of ink through a stencil screen (e.g., fabrics) on the desired substrates. **Figure 5a** shows

a typical process of screen printing, where a template mask allows ink to flow through.¹²⁶ Ink formulation typically requires high ink viscosities, and thus polymeric binders are often used. Polymers, such as ethyl cellulose, polyaniline,¹²⁷ and polyvinyl alcohol,¹²⁸ have been successfully demonstrated for screen-printing processes. As early as 2016, Zhang's group reported screen-printed TE devices using Bi_2Te_3 -based inks with Disperbyk-110 (phosphoric acid polyester based additive) as a binder (**Figure 5b-c**).¹⁰² The films showed a peak zT of 0.43 at 175 °C and good mechanical stability evidenced by 150 bending cycles.

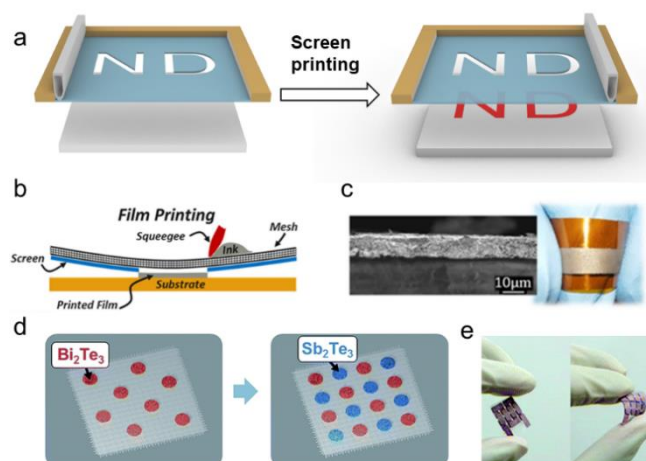


Figure 5. Screen printing and its application in fabricating TE devices. (a) Schematic of a typical screen-printing process. (b) Screen printing process of flexible TE films using $\text{Bi}_2\text{Te}_{2.8}\text{Se}_{0.2}$ nanoplate ink. (c) Cross-section SEM image and optical image of printed $\text{Bi}_2\text{Te}_{2.8}\text{Se}_{0.2}$ film.¹⁰² (d) Schematic of the screen-printed Bi_2Te_3 and Sb_2Te_3 on glass fabrics. (e) Optical image of flexible

screen-printed TE devices.¹²⁹ b-c) Adapted from ref. 102 with permission from Springer Nature. d-e) Adapted from ref. 129 with permission from RSC.

Screen printed TE devices have shown exceptional adaptability to arbitrary geometries of heat source surfaces. Several flexible devices on Kapton substrates were demonstrated using pastes of well-established TE materials.^{130, 131} Inorganic Bi_2Te_3 and Sb_2Te_3 , combined with organic PEDOT:PSS, showed zT values around 0.2 and 0.4 after a chemical treatment.¹¹⁰ Although an organic binder improves the processability of TE ink in screen printing, it typically decreases the electrical conductivity of the TE particles, and a sintering step is required to improve functionality. However, unlike bulk TE pellets, the flexible TE films are more vulnerable to oxidation and possible sublimation. Kim et al. found that introducing excess tellurium powder into the sintering chamber may alleviate the above side reaction during thermal annealing. The authors found that the carrier mobility of a screen printed Sb_2Te_3 thick film was increased threefold, and the power factor nearly doubled, resulting in a zT of 0.32. Screen printing has also been used for fabricating flexible and wearable thermoelectric devices (**Figure 5d-e**).¹²⁹ Such flexible TE devices are relatively thin and light in weight ($\sim 0.13 \text{ g cm}^{-2}$), which is important for harvesting human body heat. The TE devices also showed good thermoelectric performance even at low temperature difference with output power per unit weight of 28 mW g^{-1} .¹²⁹

4.2. Inkjet printing

Inkjet printing is a versatile manufacturing technique performed by jetting discrete ink droplets through a nozzle. **Figure 6a** shows an inkjet printing process which is based on a pressurization actuator (thermal, piezoelectric, etc.) to eject a stream of ink droplets that contains materials of interest.¹³² Nozzles of inkjet printing are typically $10\text{--}30 \mu\text{m}$ in diameter, and droplet volume is typically in the range of $1\text{--}20 \text{ pL}$. Inkjet printing typically involves inks with low viscosity ($1\text{--}50 \text{ cP}$), and the stable jetting of an ink can be estimated by a dimensionless Z number which describes the ink fluidic properties.^{133, 134} For a given printer nozzle (nozzle diameter of D), the relationship between the Z number with ink density (ρ), surface tension (γ), viscosity (η), and Ohnesorge number (Oh) can be shown as follows.³⁵

$$Z = \frac{1}{Oh} = \frac{\sqrt{\gamma\rho D}}{\eta}$$

As a rule of thumb, an ink with Z number of $1\text{--}14$ indicates stable ink jetting.^{135, 136} Ink with $Z > 14$ may form satellite droplets, while $Z < 1$ indicates elongated ligaments which may also break up into satellite droplets.³⁵

Owing to its high spatial resolution, inkjet printing of thermoelectric materials has attracted increasing research attention over the past decade. For example, Juntunen et al. reported flexible p-type graphene thin films by inkjet printing.¹³⁷ A graphene-based ink was prepared using liquid-phase exfoliation and can be readily printed into various patterns (**Figure 6b**). As shown in **Figure 6c**, the inkjet-printed graphene on polyimide is fairly flexible and is thus suitable for conforming onto nonplanar hot surfaces. Due to the moderate Seebeck coefficient of graphene ($\approx 41 \mu\text{V K}^{-1}$), the printed TE

films show a room-temperature thermoelectric power factor of $18.7 \mu\text{W m}^{-1} \text{K}^{-2}$. Despite the high thermal conductivity of CVD-grown graphene, the authors introduced disordered nanoporous structures in few-layer graphene films, leading to some degree of phonon-glass character and a relatively low thermal conductivity of $1.00 \pm 0.25 \text{ W m}^{-1} \text{K}^{-1}$. Sb-Bi-Te-Se alloys have also been printed using inkjet printing techniques. Inks of $\text{Sb}_{1.5}\text{Bi}_{0.5}\text{Te}_3$ and $\text{Bi}_2\text{Te}_{2.7}\text{Se}_{0.3}$ have been printed followed by thermal sintering in Ar/ H_2 environment.¹²² The authors reported a moderate power factor for $\text{Sb}_{1.5}\text{Bi}_{0.5}\text{Te}_3$ ($77 \mu\text{W m}^{-1} \text{K}^{-2}$) and $\text{Bi}_2\text{Te}_{2.7}\text{Se}_{0.3}$ ($183 \mu\text{W m}^{-1} \text{K}^{-2}$). As another example, Chen et al. developed printable inks of Bi_2Te_3 and $\text{Bi}_{0.5}\text{Sb}_{1.5}\text{Te}_3$ nanowires using a solution-phase synthesis method, where thermal sintering is also applied after printing. During the high-temperature thermal annealing ($450 \text{ }^\circ\text{C}$), the printed TE nanomaterials' morphology changed from a nanowire shape to a microdisk form (**Figure 6d**). Thanks to the optimization of sintering parameters, the maximum power factor for the Bi_2Te_3 and $\text{Bi}_{0.5}\text{Sb}_{1.5}\text{Te}_3$ are $180 \mu\text{W m}^{-1} \text{K}^{-2}$ and $110 \mu\text{W m}^{-1} \text{K}^{-2}$, respectively. As shown in **Figure 6e-f**, a TE prototype that harvests waste heat from hot water was developed. Despite the small temperature difference between the water and the air, a measured voltage of 9.8 mV was demonstrated.¹³

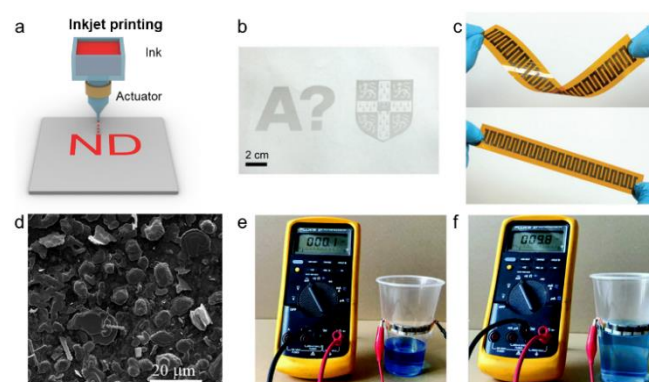


Figure 6. Inkjet printing and inkjet-printed TE materials. (a) Schematic of inkjet printing process. (b) Printed pattern of thermoelectric graphene. (c) Printed TE legs of graphene.¹³⁷ (d) SEM image of inkjet-printed TE particles annealed at $450 \text{ }^\circ\text{C}$. (e-f) Photographs of a flexible TEG prototype tapped on water cup, showing open circuit voltage before (e) and after adding enough hot water in cup (f).¹³ b-d) Adapted from ref. 137 with permission from Wiley-VCH. e-f) Adapted from ref. 13 with permission from RSC.

In addition to inorganic thermoelectric particles, organic TE polymers have also shown encouraging potential for inkjet-printed TE devices. As inkjet printing requires less viscous inks in comparison with screen printing, polymer systems with lower viscosity, such as PEDOT, have been successfully demonstrated. Inkjet printing of a TE module with p-type legs of PEDOT-tosylate (Tos) and n-type legs of tetrathiafulvalene-tetracyanoquinodimethane (TTF-TCNQ) was demonstrated with decent power output ($0.128 \mu\text{W}$).¹³⁸ The power factor of PEDOT-Tos was further tuned by adjusting the oxidation level.

With the oxidation level changed from 36% to 15%, the polymer conductivity decreased significantly (300 S cm^{-1} to $6 \times 10^{-4} \text{ S cm}^{-1}$). To better improve the ink dispersity and printability, ball milling was used to prepare inks of poly[Cu_x(Cu-ett)]/Poly(vinylidene fluoride) (PVDF)/dimethyl sulfoxide and poly[K_x(Ni-ett)]/PVDF/*N*-methyl-2-pyrrolidone.¹⁰⁷ The authors reported PF of 1.92 and $1.58 \mu\text{W m}^{-1}\text{K}^{-2}$ for n-type and p-type materials, respectively. An output voltage of 15 mV was obtained for a temperature difference of 25 K.¹⁰⁷

4.3. Aerosol-jet printing

The aerosol jet printing is an emerging printing technique that is based on the reliable transfer of focused aerosolized droplets onto substrates.¹³⁹⁻¹⁴² This approach begins with aerosolizing TE inks with sonication force or shear pressure, forming a dense stream of aerosolized droplets (**Figure 7a**). Aerosol jet printing can handle inks with broad range of viscosity from 1 cP to approximately 1000 cP, which is much more general than conventional inkjet printing (5–50 cP).⁷ With appropriate ink formulation, the printed line width can be controlled to be as low as 10 μm .¹⁴³ Recently, aerosol jet printing has been used to print a wide range of materials onto various surfaces.¹⁴⁴⁻¹⁴⁸ In particular, aerosol jet printing can print on a curved substrate, such as 3D cylindrical pipes, as the print head is able to move freely in 3D space and can work relatively far from the desired surface ($\sim\text{cm}$).

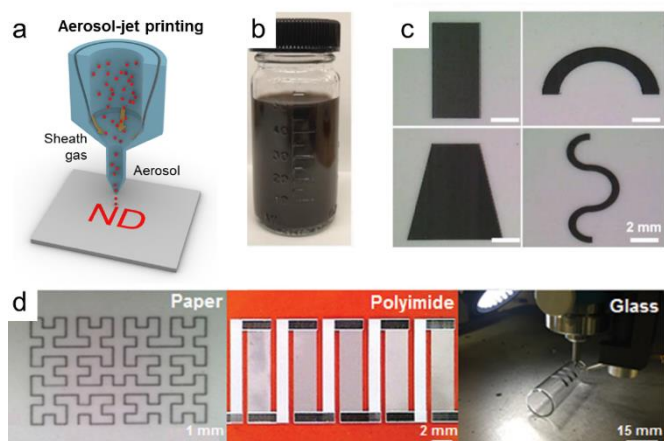


Figure 7. Aerosol-jet printing and printed TE materials. (a) The working principle of aerosol-jet printing. (b) Camera images of thermoelectric inks for aerosol jet printing. (c) Several printed patterns of TE inks using aerosol jet printing.¹⁰⁴ (d) The as-printed films with designed patterns printed on various 2D and 3D substrates.¹⁰³ b-c) Adapted from ref. 104 with permission from Wiley-VCH. d) Adapted from ref. 103 with permission from Wiley-VCH.

The ability of aerosol jet printing to process inks with a wide range of viscosity greatly expands the choice of ink materials including metals, semiconductors, and polymers.^{7, 149} This feature can be particularly helpful for printing nanocomposites of multiple materials with distinct shapes and morphology. For example, Zhang's lab has demonstrated the printing of shape-versatile TE composite of Sb_2Te_3 nanoplates with Te nanorods

(**Figure 7b-c**).¹⁰⁴ The printed TE device showed a maximum power factor of $2.2 \text{ mW m}^{-1}\text{K}^{-2}$ at 500 K and a competitive electrical power density of 7.65 mW cm^{-2} on a flexible device at 60 K temperature difference. The printed film demonstrated high flexibility with only a slight increase of 0.6% in resistance after 1000 bending cycles (curvature radius at 7 mm). Organic polymers and inorganic particles have also been demonstrated using aerosol jet printing. Recently, different organic and/or inorganic composites, including CNTs-PEDOT:PSS and Sb_2Te_3 -CNTs-PVP-PEDOT:PSS, were fabricated by aerosol-jet printing.¹⁰⁵ The authors also compared and studied the different loading ratios of Sb_2Te_3 and MWCNTs within the PEDOT:PSS matrix. In addition to the homogeneous mixing of polymer and inorganic nanoparticles, the same group also developed compositionally graded thermoelectric composites to optimize the PF along the applied temperature gradient.¹⁵⁰ Under a temperature difference of 70 K, the authors found that the 15 wt% Bi_2Te_3 -PEDOT:PSS nanocomposite showed an enhanced power output $\approx 13 \text{ nW}$, while the p-type leg comprising 50 wt% Sb_2Te_3 -PEDOT:PSS nanocomposite showed a power output of $\approx 10 \text{ nW}$. Recently, solution-processed $\text{Bi}_2\text{Te}_{2.7}\text{Se}_{0.3}$ was also printed on various substrates using the aerosol jet printing technique.¹⁰³ As shown in **Figure 7d**, both 2D and 3D substrates were used with high spatial resolution. The aerosol jet printed $\text{Bi}_2\text{Te}_{2.7}\text{Se}_{0.3}$ films demonstrate a room-temperature power factor of $730 \mu\text{W m}^{-1}\text{K}^{-2}$ using a rapid photonic sintering technique.¹⁰³

4.4. Extrusion-based printing

Extrusion-based printing, such as dispenser printing, is a popular strategy for 2D and 3D printing of nanomaterials due to its low cost, ease of use, and wide material options. Extrusion printing relies on the external pressure (induced by piston, pressurized air, or screw force) which pushes the ink to form 3D objects followed by a solidification process.²³ The printing resolution of the dispenser printing is often controlled or closely related to the nozzle size.^{151, 152} An important feature of dispenser printing is the wide material choice because it can handle not only low-viscosity particle dispersions, but also exceedingly viscous inks with large particle loading. This advantage of dispenser printing enables numerous ink options, and thus a wide range of nanomaterials have been successfully printed using dispenser printing.¹⁵³⁻¹⁵⁵ The viscoelastic properties of some inks have allowed self-supporting structures,^{153, 156} which can be particularly useful for fabricating functional devices with relatively large thickness.¹⁵⁷⁻¹⁶⁰

A typical extrusion/dispenser printing of thermoelectric materials is shown in **Figure 8a**. Jung et al. demonstrated a flexible solar thermoelectric generator by dispenser printing of $\text{Bi}_{0.4}\text{Sb}_{1.6}\text{Te}_3$ and $\text{Bi}_2\text{Se}_{0.3}\text{Te}_{2.7}$.¹⁶¹ As shown in **Figure 8b**, various patterns of TE ink are dispenser printed on a flexible polyimide substrate. After depositing five layers of solar absorber using Ti/MgF₂, the solar thermoelectric generator comprising 10 pairs of p-n legs has an open-circuit voltage of 55.15 mV. Park et al. designed a bracelet-type TE device where CNT is deposited on a flexible substrate.¹⁶² The bracelet-type TE device with 60 pairs of n- and p-doped CNT exhibits a maximum power output of

1.95 μW at 30 K temperature difference. The printed CNT devices possess high flexibility with minimal resistance change after more than 3000 bending cycles. This flexible TEG could be useful for harvesting energy on curved heat sources.

As extrusion printing can work with relatively viscous inks, several structural polymers, such as epoxy, have been used to fabricate TE composite. For example, the Evans group demonstrated epoxy-based inks of n-type Bi_2Te_3 and p-type Sb_2Te_3 with a room temperature zT of 0.16 and 0.41, respectively.^{163, 164} The same group also developed a 50-couple prototype device with a power output of 10.5 μW at 61.3 μA and 172 mV under a temperature difference of 20 K.¹⁶⁵ Ultra-violet light curable polymers can be printed as structural materials or supporting structures, which eliminates the need for masks to transfer the patterns onto the substrate.¹⁶⁶ For example, Cao et al presents a vertically fabricated 3D thermoelectric generator by dispenser printing on flexible polyimide substrate.¹⁶⁶ This work involved the printing of electrodes, thermoelectric materials, and structural material. For a device consisting of 8 uncouples, the Seebeck coefficient and maximum power output were 23.6 $\mu\text{V K}^{-1}$ and 1.54 nW, respectively.¹⁶⁶

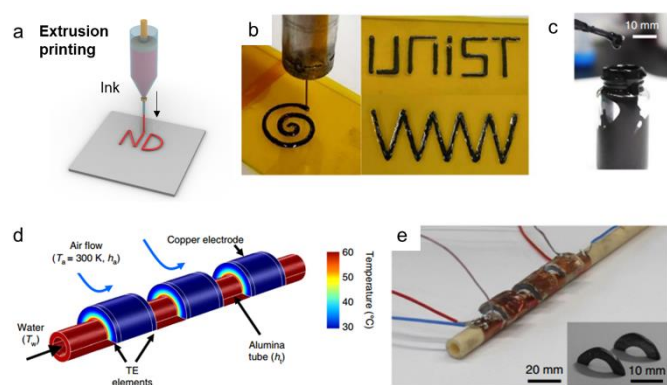


Figure 8. Extrusion printing and printed TE materials. (a) Schematic illustration of extrusion printing. (b) Extrusion printing and printed patterns.¹⁶¹ (c) Photograph of TE inks for extrusion printing. (d) Modelling of conformal printed TE devices on pipelines. (e) Optical image of printed thermoelectric generators with inset showing n-type and p-type half rings.¹¹¹ (b) Adapted from ref. 161 with permission from Elsevier. (c-e) Adapted from ref. 111 with permission from Springer Nature.

With careful design of TE ink formulation, extrusion/dispenser printing is able to build 3D devices that can be conformal on non-planar curved heat sources. Son's group developed a cylindrical TE device that can be directly attached onto an alumina tube conformally, using a dispenser-based 3D printing process (**Figure 8c-e**).¹¹¹ The authors calculated the temperature and electrical potential distributions in the TEGs under a flow of hot water through the curved pipe and found a larger temperature gradient within the conformal TE elements and less parasitic heat loss than non-conformal planar TEGs (**Figure 8d**). As shown in **Figure 8e**, the printed device was highly compatible with curved surfaces to effectively transfer heat

energy. The inner diameter of the half-ring TE legs was controlled to match the outer diameter of the curved pipe. Owing to the use of molecular metal chalcogenide complex as a ligand and thermoelectric filler, a maximum output power of 1.62 mW (power density of 1.42 mW cm^{-2}) was demonstrated at a 39 K temperature difference.

4.5. Roll-to-roll (R2R) printing

Roll-to-roll (R2R) printing techniques (such as gravure and flexographic printing) have been widely adopted as a commercial printing technology for scale-up manufacturing of labels, smart packaging, and organic light-emitting diodes.^{167, 168} R2R printing uses predesigned plastic/metal cylinders that transfer inks onto substrates, which can be operated at fast speed and thus enables a high-throughput continuous process.¹⁶⁹ Despite some variations on process design, many R2R printing techniques allow printing procedures to be repeated several times to achieve multilayer deposition of inks. To ensure a high-resolution R2R printing, it was suggested that the small particle size would be beneficial, with which a high-resolution ($\sim 30 \mu\text{m}$) patterning of nanoparticle ink can be achieved.¹⁷⁰

By using high-throughput R2R printing, 18,000 serially connected junctions of PEDOT:PSS (6 cm^2 per junction) with top and bottom Ag electrodes were demonstrated.¹⁷¹ The architecture uses only one type of thermoelectric material (p-type) for harvesting thermal energy, which limits the power output to 54 pW at a temperature difference of 70 K.¹⁷¹ Organic interconnects are also used in roll-to-roll processing for *in situ* printing TE devices.¹¹³ Zhang *et al.* printed the inks of p-type (PEDOT:PSS), n-type (nitrogen-doped graphene), and interconnection strips (PEDOT:PSS) by three printing rollers onto a flat substrate.¹¹³ When a roller is partially immersed in corresponding inks, different conductive strips can be "stamped" on the substrates by contacting with rotating rollers followed by the solvent removing processes. The authors suggested that the solvent-borne inks of organic interconnects can dissolve some materials from the organic TE legs at the interface, which may help to lower the contact resistance for the printed devices. The authors reported a decent output power density of 0.24 mW m^{-2} at a small temperature difference of 10 K.

4.6. Spray printing and other patterned coatings

Spray printing is a popular deposition technology in art and industry, which uses pressure to spray ink through a nozzle where a large number of ink droplets are formed.¹⁷² Spray printing can enable the rapid deposition of functional ink over a large area, while several parameters (e.g., solvent, flow rate, substrate temperature) play significant roles in the uniformity of deposited films. To fabricate devices with controlled patterns, a predesigned mask is often needed to ensure the formation of desired device architectures.

Spray printing of thermoelectric materials has been investigated recently for a possible solution toward large-scale manufacturing of TE devices. For example, Hong et al. developed a flexible CNT/P3HT organic thermoelectric generator by spray-printing.¹¹² The as-prepared printed films

showed high flexibility with Seebeck coefficient, electrical conductivity, and power factor of $97 \pm 11 \mu\text{V K}^{-1}$, $345 \pm 88 \text{ S cm}^{-1}$, and $325 \pm 101 \mu\text{W m}^{-1} \text{K}^{-2}$, respectively. Bae investigated the effect of nanocarbon material in spray-printed Te-PEDOT:PSS devices using graphene and carbon nanotubes (SSWNTs).¹⁷³ During the ink formulation, Te and PEDOT:PSS were homogenized with the addition of nanocarbon. In the

presence of 0.3 wt% of SSWNTs, a power factor of $206 \mu\text{W m}^{-1} \text{K}^{-2}$ was achieved thanks to the high Seebeck coefficient of $118 \mu\text{V K}^{-1}$. The SSWNT-mixed Te-PEDOT:PSS devices showed output power of 126 nW, demonstrating a flexible and lightweight TE prototype for energy harvesting from the human body. Additional examples of various printing methods have been shown in **Table 2**.

Table 2: Common examples of printing methods and their key characteristics. *The viscosity is the typical range printable for using nanomaterials and polymers,^{7, 35} in which it may vary depending on the material type and processing design.

Printing methods	Template required	Capabilities/Features	Ink viscosity* (mPa · s)	TE examples
Screen printing	Yes	High particle load	1000–10000	Sb ₂ Te ₃ ¹²⁹ , Bi ₂ Te ₃ /PEDOT ¹²¹
Roll to roll printing	Yes	High throughput, low production cost	100–2000	PEDOT:PSS ¹⁷¹
Spray printing	Yes	Good for large devices	50-500	CNT/P3HT ¹¹²
Aerosol jet printing	No	High resolution, expanded material types	1-1000	Sb ₂ Te ₃ /Te ¹⁰⁴ , Bi ₂ Te _{2.7} Se _{0.3} ¹⁰³
Inkjet printing	No	High accuracy and uniformity, high spatial resolution	1-50	Poly[Cu _x (Cu-ett)] /PVDF ¹⁰⁷
Extrusion printing	No	Easy to print, wide viscosity range	30–10 ⁷	Bi _{0.5} Sb _{1.5} Te ₃ ¹¹¹ , Te/PEDOT ¹¹⁰

4.7. Post-printing treatment

Many nanomaterial-based inks, including thermoelectric inks, often contain organic molecules to adjust ink rheology or mitigate aggregation of the TE colloidal nanoparticles in solution. The presence of insulating organic stabilizers impedes the formation of conductive pathways which inevitably lower the overall thermoelectric properties. Therefore, post-printing sintering is useful to remove organic additives and consolidate the TE particles. Upon the removal of the surfactants at sufficiently high temperatures, the TE nanoparticles are in direct contact and thus form a percolating pathway, in which Ostwald ripening of nanoparticles occurs driven by their high surface energy.

One popular sintering approach is thermal sintering where printed materials are processed at elevated temperatures.^{174, 175} However, conventional thermal sintering requires high temperatures for relatively long durations whereas most of the cost-effective polymer substrates for printing flexible devices, such as polyethylene terephthalate (PET), polycarbonate (PC), or fabrics, have relatively low glass transition temperatures which are not compatible with traditional thermal sintering.¹⁷⁵ In addition, thermal sintering, due to its unselective heating,

limits the further development of all-printed devices from temperature-sensitive TE materials.

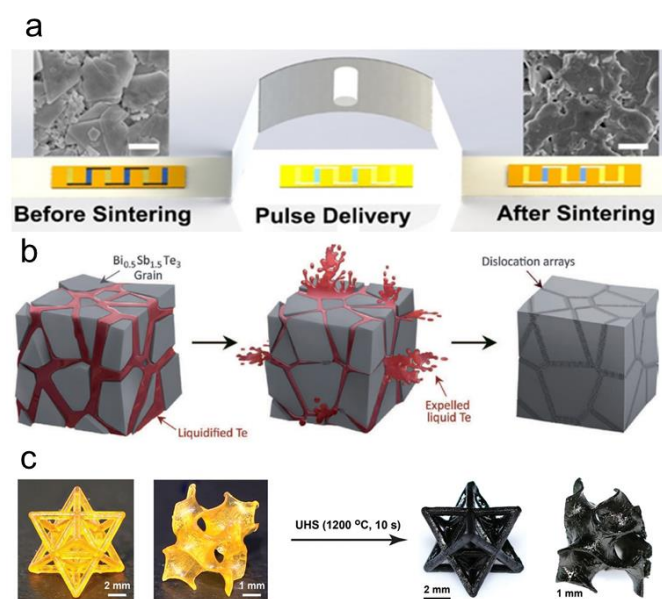


Figure 9. Various sintering and post-treatment methods. (a) Schematic illustration of intense pulsed light sintering process on printed TE films, with insert SEM images of the n-type $\text{Bi}_2\text{Te}_{2.7}\text{Se}_{0.3}$ film before and after sintering, scale bar is 500 nm. Adapted from ref. 103 with permission from Wiley-VCH. (b) Schematics show the formation of dislocation arrays within the grain boundaries of $\text{Bi}_{0.5}\text{Sb}_{1.5}\text{Te}_3$ via a melt-spun and spark plasma sintering.¹⁷⁶ (c) Schematic of the ultrafast high-temperature sintering synthesis process of 3D-printed ceramic component in ~ 10 s.¹⁷⁷ b, c) Adapted from ref. 176 and ref. 177 with permission from AAAS.

The recent sintering innovations have focused on research areas including high sintering speed, high thermal selectivity, and compatibility with temperature-sensitive substrates. To improve the electrical conductivity of printed nanomaterials while avoiding the destruction of the polymeric substrates, various sintering methods, including photonic,¹⁷⁸⁻¹⁸⁰ plasma,^{181, 182} microwave,¹⁸³⁻¹⁸⁵ and chemical sintering,^{186, 187} have been developed. These sintering techniques are more time-efficient, enabling scalable printing of thermoelectric devices. For example, Saeidi-Javash *et al.* demonstrated aerosol jet printing and photonic sintering of n-type $\text{Bi}_2\text{Te}_{2.7}\text{Se}_{0.3}$ TE films (**Figure 9a**).¹⁰³ The photonic sintering significantly improved the electrical conductivity of the printed films from non-conductive to 2.7×10^4 S/m within seconds, which led to a power factor of

$730 \mu\text{W m}^{-1}\text{K}^{-2}$ at room temperature. Recently, there have been a number of emerging sintering approaches developed for removing organic components and consolidating the particles of interest, though not all of these methods are directly used for sintering printed TE material. However, their design principles and sintering physics could be valuable for post-printing treatment of thermoelectric devices. As shown in **Figure 9b**, Kim *et al.* reported the application of spark plasma sintering for fabricating ball-milled, and stoichiometric melt-spun $\text{Bi}_{0.5}\text{Sb}_{1.5}\text{Te}_3$ TE materials.¹⁷⁶ They applied a simple liquid-phase compacting process that reduced lattice thermal conductivity to $0.33 \text{ W m}^{-1}\text{K}^{-1}$ at 320 K and resulted in an exceptionally high zT of 1.86. As shown in **Figure 9c**, Wang *et al.* introduced an ultrafast high-temperature sintering process, in which precursor powder is directly sintered into a dense ceramic component at a high sintering temperature of up to 3000 °C in ~ 10 s.¹⁷⁷ In this methodology, both pressed pellets and 3D-printed objects are sandwiched between two Joule-heating carbon strips that heat the pellets with high heating ($\sim 10^3$ to 10^4 °C/min) rate through radiation and convection. Although this method was not directly demonstrated on thermoelectric materials, it is expected that its ultrafast and high temperature features may enable the sintering of some TE oxides such as ZnO. A number of sintered p-type and n-type thermoelectric materials have been summarized with different printing methods as well as post-processing conditions in **Table 3**.

Table 3: Comparison of printed thermoelectric materials with processing methods. *The thermal conductivity data are not always readily available for printed TE materials, so the focus here is on Seebeck coefficient (S), electrical conductivity (σ), and power factor (PF).

	Materials	Fabrication	Post-treatment	S ($\mu\text{V/K}$)	σ (S/cm)	PF* ($\mu\text{W}/(\text{m}\cdot\text{K}^2)$)
P type	$\text{Sb}_{1.6}\text{Bi}_{0.4}\text{Te}_3/\text{Te}$	Screen printing	450 °C, 45 min	204	720	3000 ¹⁰¹
	Sb_2Te_3	Screen printing	500 °C, 30 min	98	1500	1441 ¹²⁹
	$\text{Bi}_{0.5}\text{Sb}_{1.5}\text{Te}_3$	Extrusion printing	450 °C, 1 h	165	554	1508 ¹¹¹
	$\text{Sb}_2\text{Te}_3/\text{epoxy}$	Extrusion printing	250 °C, 3 h	160	63	160 ¹⁶⁵
	$\text{Sb}_2\text{Te}_3/\text{Te}$	Aerosol jet printing	400 °C, 1 h	198	560	2200 ¹⁰⁴
	Te/PEDOT	Extrusion printing	120-160 °C	115	215	284 ¹¹⁰
	Poly[$\text{Cu}_x(\text{Cu-ett})$]/PVDF	Inkjet printing	363 K, 10 h	41.0	5.1	0.9 ¹⁰⁷
	SnSe/PEDOT	Drop casting	328 K, 6 h	110	320	390 ¹⁸⁸
	CNT/P3HT	Spray printing	R.T.	97	345	325 ¹¹²
	CNT/PANI	Drop casting	40–50 °C, 20 h	61	610	220 ¹⁸⁹
Graphene/PANI	Drop casting	40 °C	26	814	55 ¹⁹⁰	
N type	Bi_2Te_3	Screen printing	530 °C, 10 min	-141	670	1332 ¹²⁹

ARTICLE

Journal Name

$\text{Bi}_2\text{Te}_{2.8}\text{Se}_{0.2}$	Screen printing	430 °C	-126	310	490 ¹⁰²
$\text{Bi}_2\text{Te}_3/\text{PEDOT}$	Screen printing	450 °C	-138	73	138.6 ¹²¹
$\text{Bi}_2\text{Te}_3/\text{epoxy}$	Extrusion printing	250 °C, 3 h	-157	61	150 ¹⁶⁵
$\text{Bi}_2\text{S}_3/\text{PANI}$	Drop casting	483 K, 10 min	-42.8	0.4	0.07 ¹⁹¹
Poly[K _x (Ni-ett)] /PVDF	Inkjet printing	363 K, 10 h	-44.9	2.1	0.4 ¹⁰⁷
$\text{V}_2\text{O}_5/\text{PEDOT}$	Inkjet printing	100 °C, overnight	-350	0.16	2 ¹⁰⁶
$\text{Bi}_2\text{Te}_3/\text{Se}/\text{epoxy}$	Extrusion printing	250/350 °C, 12 h	-170	96	277 ¹⁰⁹
$\text{Bi}_2\text{Te}_{2.7}\text{Se}_{0.3}$	Aerosol jet printing	Photonic sintering, 1.5 s	-163	270	730 ¹⁰³
$\text{TiS}_2(\text{HA})_x$	Inkjet printing	110 °C	-70	430	211 ¹⁰⁸

5. Development of conformal/flexible TE devices

Due to the ability to closely interface with uneven surfaces such as a pipeline or human body, conformable/flexible TE devices offer unique advantages for innovative applications far beyond their rigid counterparts. To date, although several flexible and stretchable TEGs adapted to curved surfaces have been demonstrated, the development of defect-free self-standing devices for irregular surfaces remains underexplored. This section will discuss the principle of conformal and flexible designs and critically review recent advances in conformal/flexible fabrication techniques. Although not all conformal/flexible design strategies are based on thermoelectric materials, this section strives to cover versatile design strategies that may be applicable to TE devices.

5.1. Conformal devices

Conformability is the capability of mechanical adaptivity that can be attached to arbitrary curvilinear surfaces.¹³² For conformal TE devices, studies suggest a significantly larger temperature gradient within the conformal TE elements and less parasitic heat loss than non-conformal planar TEGs due to improved heat transfer at the interfaces.¹¹¹ The conformability of a device can be investigated at two levels: 1) for the overall profile and 2) for small wrinkling. It was suggested that the interface mechanics and soft adhesion at the interface dictate the nature of this contact.¹⁹² **Figure 10a** presents a conformal contact between a thin silicone and a uneven surface (skins), indicating that a thinner material system may lead to better conformal contact on an irregular surface.¹⁹³ For example, past works showed that the critical thickness for skin conformal contact is ~ 25 μm for substrates of elastic moduli <0.1 MPa.¹⁹³ Further, 2D conformability of stretchable electronics has been studied with various thicknesses of substrates, coverage areas, and external loadings.¹³² Due to the low bending stiffness, stretchable devices typically show good conformal contact to a curved surface. It was suggested that the extent of conformal coverage increases with decreasing thickness in devices for uneven surfaces,¹⁹⁴ while the formation of conformal devices

can be expanded if in situ fabrication (*e.g.*, conformal printing) is available for building devices based on substrate geometry.

The strategies to integrate devices on complex substrates (*e.g.*, skin and engine) include direct ink deposition,¹⁵² temporary epidermal tattoos,¹⁹⁵ hard-soft integration,¹⁹⁶ and functional substrates.¹⁹⁷ As shown in **Figure 10b**, the direct deposition of ink material by a non-contact printing method leads to the rapid fabrication of a conformal electronic device.¹⁴³ The printing resolution of the direct ink deposition is normally determined by the size of printing nozzles and the ink rheology, where these ink/printing parameters can be used for designing and fabricating conformal electronics and optoelectronics.^{151, 152} In addition, conformal devices can be obtained by attaching flexible devices onto application-specific substrates. Inspired by the concept of a temporary tattoo, conformal electronics leverage flexible polymers to enable good conformal contact.¹⁹⁸ The fabricated electronic tattoos were then laminated on the desired object for applications. Various polymers including polyethylene terephthalate,¹⁹⁹ poly(vinyl alcohol),²⁰⁰ and water-soluble tapes¹⁹⁷ have been used as supporting layers for mounting electronic patterns on the substrates, enabling the development of a number of conformal sensors and functional devices. As shown in **Figure 10c**, silver ink was first printed on an A4-sized PVA substrate, forming conductive interconnects. Taking advantage of water-soluble feature of PVA, the authors demonstrated that the printed patterns can be easily wrapped around random 3D shapes, such as a 3D-printed model car (**Figure 10d**).²⁰¹ The conformal design has been investigated in several thermoelectric systems.^{31, 202-204} For example, p-type $\text{Sb}_2\text{Te}_3\text{-Te}$ nanoparticles have been directly printed on curved surfaces to form conformal TE patterns and devices (**Figure 10e**). At a ΔT of 60 K, the device demonstrated a maximum power output of 1.15 μW and an excellent power density of 7.65 mW cm⁻² (**Figure 10f-g**), which can be attributed to the high Seebeck coefficient of $\text{Sb}_2\text{Te}_3\text{-Te}$ nanocomposites.

ARTICLE

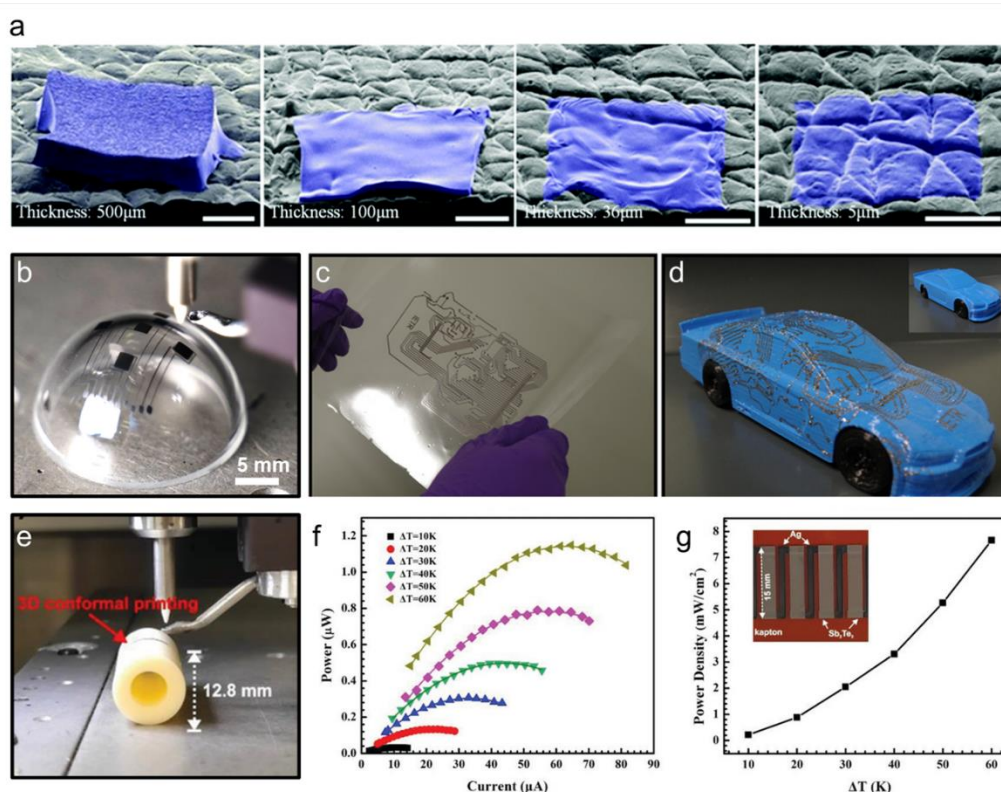


Figure 10. Conformal design in printed devices. (a) Different degree of conformal contact between a silicone replica of the surface of the skin (grey) and various thicknesses of elastomer membrane substrates (blue).¹⁹³ (b) Photograph of a conformal antenna during the printing process.¹⁴³ (c) Printed Ag interconnects on removable substrate. (d) Printed Ag interconnects transferred on 3D objects.²⁰¹ (e) Printed thermoelectric devices that are conformal to curved surfaces. (f) Device power output versus electrical current. (g) Power density tested at different ΔT (Inset: photo of the thin-film TE device).¹⁰⁴ a, b, e-g) Adapted from ref. 193, ref. 143 and ref. 104 with permission from Wiley-VCH. c-d) Adapted from ref. 201 with permission from ACS.

5.2. Flexible and stretchable devices

The development of flexible and stretchable devices has provided a promising solution to meet the increasingly stringent design constraints of heat sources with complex geometries (e.g. human body).^{205, 206} **Figure 11a** provides an overview of materials with different stiffness (elastic modulus).^{207, 208} The supporting and encapsulating polymers show elastic moduli close to that of the biological systems, while being significantly different from electronic materials (e.g. metals). Structural design of the device layouts and development of assembly schemes for the active layers are promising strategies to mitigate the mechanical mismatch between functional materials and substrates.

The flexibility of a device can be defined as $1/r_b$, where r_b indicates the minimum bending radius of curvature.²⁰⁹ The

minimum bending radius depends on material properties (e.g., yield stress and Young's modulus) as well as device thickness. Thus, a simple strategy to fabricate devices with high flexibility involves implementing low thickness. As shown in **Figure 11b**, the relatively small thickness of the device enables a flexible transistor to bend around a hair.²¹⁰ In fact, printing and thin-film technology allow the fabrication of ultrathin polymers, metals, and semiconducting materials to produce active electronic devices of sub-micron thickness. For example, highly bendable electronics based on silicon²¹¹ were realized as early as 2008. Past studies have reported approaches to manufacture large-area devices on ultrathin substrates, thus allowing bending radii as small as tens of microns.^{212, 213} In addition, a judicious selection of materials with strong mechanical stability, such as PEDOT,^{49, 52} carbon nanotubes²¹⁴ and graphene,^{215, 216} is

another important approach for the fabrication of highly flexible devices.

Encapsulation techniques are an emerging approach to promote device flexibility and stability, which allows the active layers positioning at a zero-strain plane.²¹⁷ A mechanical neutral plane (MNP) approach, where stress and strain are zero during bending, is frequently adopted through placing the brittle functional thin film close to the MNP (**Figure 11c-d**).²¹⁸ Studies showed that an MNP design enables field-effect transistors to survive after 60000 bending cycles due to reduced strain-induced damage.²¹⁹ Likewise, multilayered structures with soft

interlayers can reduce deleterious interactions among the hard layers inside devices. MNP can be divided into several planes, protecting brittle layers at multiple locations during bending cycles.²²⁰ Theoretical works revealed that such splitting of MNP relies on the thickness of the intermediate layer as well as the length-to-thickness ratio of the multilayers.^{221, 222} Finite element method analyses have been proposed to guide the device designs when employing MNPs.²²³

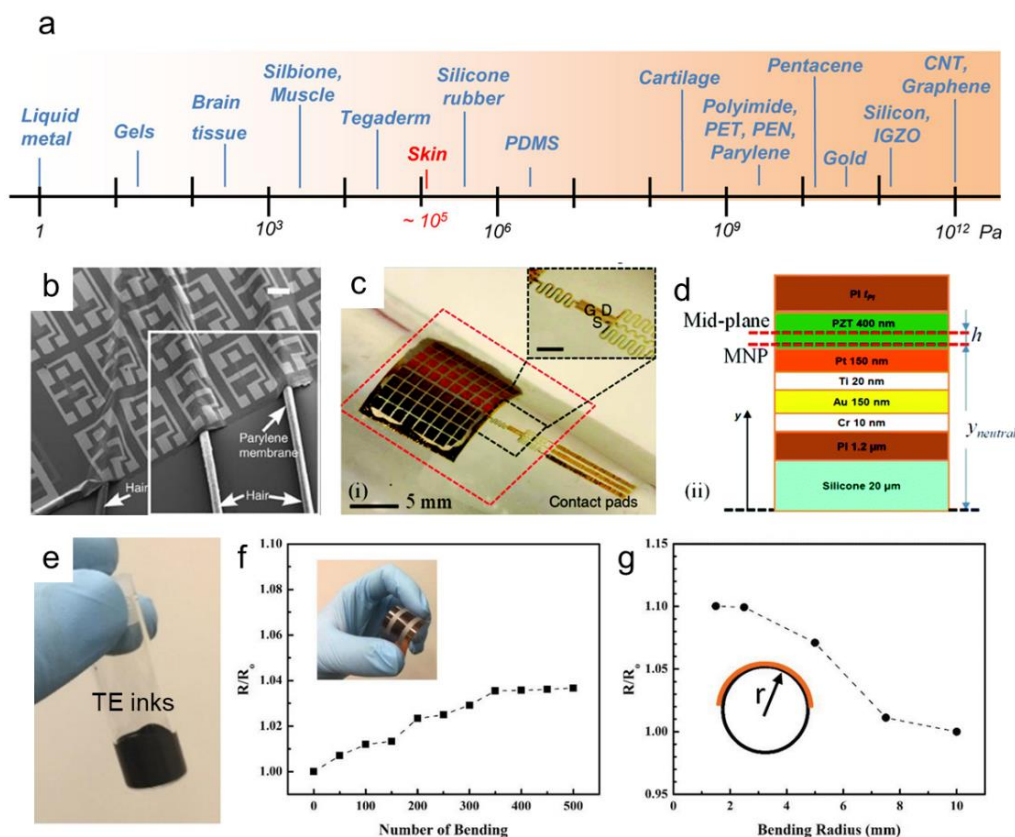


Figure 11. Device design of flexible electronics. (a) Elastic moduli of common materials.²⁰⁷ (b) SEM image of flexible thin-film transistors on hairs, showing high flexibility.²¹⁰ Scale bar: 200 μ m. (c) Image of a device wrapped on a cylindrical glass support. (d) Schematic of a sensor on a silicone substrate with mechanical neutral plane (MNP) strategy. (e) Optical image of printable TE inks. (f) Resistance changes of printed flexible TE films at different bending cycles. (g) Resistance change under different bending radius.¹⁰³ a) Adapted from ref. 207 with permission from ACS. b-d) Adapted from ref. 210 and ref. 218 with permission from Springer Nature. e-g) Adapted from ref. 103 with permission from Wiley-VCH.

Printing techniques have provided a facile approach for fabricating flexible TE devices. For example, studies showed that non-contact printing approaches can readily convert thermoelectric inks of Bi₂Te_{2.7}Se_{0.3} (**Figure 11e**) into flexible devices.¹⁰³ Due to the low thickness controlled by printing processes, the printed thermoelectric devices showed high mechanical flexibility and stability. As shown in **Figure 11f**, only a slight change (4%) in film resistance was seen after 500 bending cycles. Flexibility tests at a number of bending radii revealed insignificant resistance change (<10%) in electrical

resistance even at a small bending radius of 1.5 mm (**Figure 11g**).

Stretchability is another important element for realizing broad device applications, such as epidermal TE devices. For instance, an ideal wearable TE device should not only demonstrate high flexibility that allows them to conform to the human body but also show stretchability to accommodate strains during daily motion. Various spring-like structures, such as mesh and serpentine structures, can be used for fabricating stretchable devices. A semiconducting network with a honeycomb mesh structure has been demonstrated on

polyimide substrates.²²⁴ A great number of mesh-based structures have enabled stretchability on the device level. For example, Guo *et al.* showed a gold nanomesh with no fatigue after 50,000 stretches to a strain up to 150% (**Figure 12a**).²²⁵ Miyamoto *et al.* demonstrated a stretchable sensor from a mesh network design, in which on-skin sensors can decrease the risk of inflammation.²²⁶ **Figure 12b-c** shows various serpentine designs which help to improve the stretchability of devices.^{195, 227-229} For example, a 3D buckled ribbon structure offers a promising solution for stretchable semiconductors (**Figure 12c**).²³⁰ Remarkably, Roger's group successfully fabricated a deformable and semitransparent display based on microscale inorganic light-emitting diodes.²³¹ In addition, **Figure 12d** shows a stretchable "island-bridge" design that connects conductive traces (bridges) with rigid functional modules (islands).²³² The conductive bridge provides low effective stiffness and therefore accommodates the stretching of the entire device while decreasing strains in rigid modules (such as rigid TE components).

Packaging electronic components in low-modulus materials is another approach to form stretchable devices. An ideal package should minimize possible constraints on the objects (such as a human body).²³³⁻²³⁵ For this type of stretchable device, one strategy utilizes a core/shell package where a core with an ultralow elastic modulus is packaged in a silicone shell, as shown in **Figure 12e**.²³⁵ As an extreme example, rigid functional devices can be integrated with liquid-filled packaging structures to form strain-isolation layers. With appropriate design and material choice, these approaches may also enable mechanically robust soft TE devices. For example, Yang *et al.* fabricated stretchable thermoelectric devices by integrating TE arrays and serpentine interconnects (**Figure 12f**). In this type of stretchable TEG (S-TEG), rigid Sb_2Te_3 and Bi_2Te_3 are used as p-type and n-type materials, respectively. By integrating 50 pairs of TE elements in stretchable silicone encapsulation, the device demonstrated an output power of 0.15 mW/cm² at a temperature difference of 19 K.

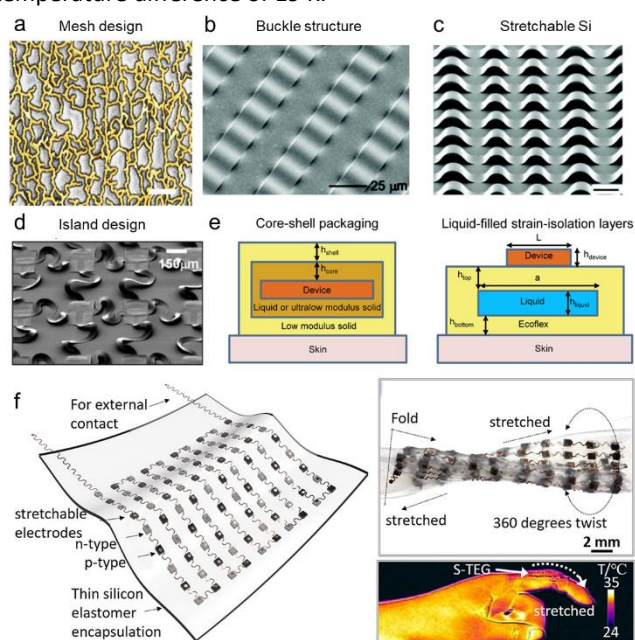


Figure 12. Device design of stretchable devices. (a) A stretchable gold electrode with a nanomesh structure.²²⁵ Scale bars: 1 μm . (b) Si ribbon fully bonded on PDMS substrates. Reproduced with permission.²²⁹ (c) Si ribbon partially bonded on a PDMS substrate.²³⁰ Scale bars: 100 μm . (d) Island-bridge stretchable electronics with serpentine interconnects.²³² (e) Cross-sectional schematic of a core-shell package for strain isolation of electronic devices (left) and a liquid-filled cavity package for strain-isolation of electronic devices (right).^{207, 235} (f) Stretchable thermoelectric devices by integrating TE arrays and serpentine interconnects, leading to a high-performance wearable TEG.²³⁶ a) Adapted from ref. 225 with permission from ACS. b) Adapted from ref. 229 with permission from AAAS. c) Adapted from ref. 230 with permission from Springer Nature. d) Adapted from ref. 232 with permission from National Academy of Sciences. e) Adapted from ref. 207, 235 with permission from Wiley-VCH. f) Adapted from ref. 236 with permission from ACS.

6. Device applications

The principles of the thermoelectric phenomenon including the direct conversion of thermal energy into electricity (Seebeck effect) or inversely from electrical current into heat flow (Peltier effect) have led to research breakthroughs in the development of thermoelectric devices. Up to date, a wide range of thermoelectric devices have been designed and developed ranging from energy harvesting to thermal management. In this section, we review the state-of-art development of TE devices for mainly energy and thermal applications, consisting of TE-based energy devices (waste heat recovery, wearable electronics, and energy harvesting from solar and nuclear sources) and thermal devices (such as TE cooler and temperature sensing).

6.1. Energy harvesting devices

A thermoelectric generator is a device that harnesses thermal energy and converts it into electricity. Unlike traditional heat engines in which the working fluid provides conversion of thermal energy to kinetic energy, a typical TEG utilizes charge carriers as the "working fluid" to directly convert heat into electricity without moving parts. Recently, the TEG has emerged as a "zero-emission" and reliable power source which is able to meet various power requirements.^{237, 238} Flexible, low-cost and reliable TEG systems are an attractive alternative for replacing batteries in various applications.²³⁹⁻²⁴¹

6.1.1 Waste heat recovery

Waste heat is defined as thermal energy generated as a side product without actual utility in the energy systems. For example, the efficiency of most combustion engines is less than 30% because of the excessive waste heat generated in the entire system.^{242, 243} To increase the efficiency of the overall system, the waste heat should be harvested by thermoelectric devices to produce electricity. Generating electrical power by recovering low-grade waste heat at temperatures < 413 K represents a significant market for TEGs. For a typical automobile, the temperature of exhaust gas can be as high as 1073 K after combustion and remains above 500 K even in the

downstream areas,^{244, 245} providing the heat source for thermoelectric devices in the intermediate to high-temperature range. As shown in **Figure 13a**, Zhang et al. demonstrated a high-performance 1 kW TE system for automotive waste heat recovery.²⁴⁶ The authors used nanostructured TE materials to fabricate devices with the power density of 5.26 W cm^{-2} at a temperature difference of 500 K. That TEG system was a proof-of-concept prototype harvesting the exhaust waste heat of a diesel engine where a heat-to-electricity efficiency of 2.1% was demonstrated. As another example, a flexible planar TEG was demonstrated and can extract heat from industrial heat pipes to power a wireless sensor network.²⁴⁷ TE devices of 420 Ag/Ni thermocouples were fabricated on flexible substrates using screen printing so that the device can adapt to the cylindrical form of the pipe. The TEG demonstrated an output power of $308 \mu\text{W}$ at a temperature difference of 127 K. Similar to screen printing, extrusion-based dispenser printing was also employed to fabricate flexible thermoelectric generators for use on low levels of waste heat.²⁴⁸ The TE elements need to be printed with optimal thickness and thermal resistance to sustain a large temperature gradient across the TE devices.

For an exhaust TEG, a conformal contact between TE elements and heat sources is essential to maximize the heat transfer and improve the overall heat-to-electricity efficiency. Conventional fabrication approaches limit the development of conformal devices with sophisticated 3D designs. State-of-the-art, non-contact printing is an effective approach to realize conformal fabrication. Recently, printing devices based on heat source geometry (such as conformal deposition of TE ink on a hemisphere²⁴⁹) have been increasingly investigated to promote effective heat transfer. Alternatively, flexible TE devices, such as thin-film TEG,²⁵⁰ can be attached to the heat source conformally to promote heat transfer. For example, a prototype TEG device is demonstrated with 525 screen-printed Ag-Ni junctions (**Figure 13b**).²⁵¹ With a Seebeck coefficient of $8.6 \mu\text{V}/^\circ\text{C}$, the open-circuit voltage for the entire device was 741 mV at a temperature difference of 165 K, and the power generated with matching load resistance was 0.28 mW, demonstrating potential market opportunity in industrial pipe energy harvesting.

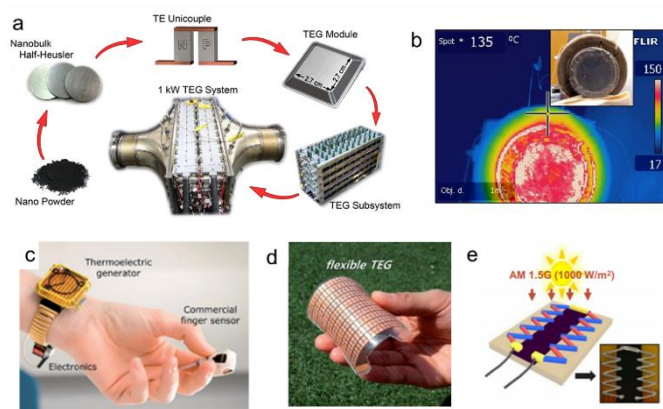


Figure 13. Examples of TE-based heat harvesting devices. (a) Schematic illustration of a 1kW TE system for waste heat

harvesting from cars.²⁴⁶ Adapted from ref. 246 with permission from Elsevier. (b) Infrared camera image of printed conformal TE devices on heat pipes. The inset shows the optical image of TE prototypes.²⁵¹ Adapted from ref. 251 with permission from TechConnect Publishing. (c) TEG-powered wearable pulse oximeter.²⁵² Adapted from ref. 252 with permission from AIP Publishing. (d) A photo of the flexible TEG product.²⁵³ Adapted from ref. 253 with permission from ACS. (e) Working principle of a printed STEG under solar radiation with the inset of TE legs.¹⁶¹ Adapted from ref. 161 with permission from Elsevier.

6.1.2 Energy harvesting from the human body

TE-based energy harvesting from the human body can be particularly important for wearable and biomedical devices.²⁵⁴ To circumvent complex wiring for power supply or battery charging, implantable TEGs are considered suitable power alternatives for implantable medical devices.²⁵² For example, implantable medical devices and wearable biomedical devices would all benefit from a self-powering feature. The electrical power required by implantable/wearable devices can be as low as sub-milliwatts,²⁵⁵ which is achievable by integrating TEGs in those devices. These integrated TEGs utilize the heat source either from the body or the skin surface, and several positions to integrate a wearable TEG to the human body were investigated using the temperature difference between the skin surface and the ambient temperature, such as upper arm, wrist, chest, an office-style shirt, or a bicycle helmet.^{252, 256, 257} However, constructing wearable TEGs faces a few challenges primarily because of the low zT values of thermoelectric materials that are compatible with biomedical applications¹²³ and the small temperature gradient across the active layer in the TEG device.²⁵⁸ In addition, a lightweight and comfortable TEG construction, including the heat exchanger, is typically required. All these constraints significantly affect the output power of the integrated TEGs. To address the issues of poor flexibility and heavyweight, the printing of lightweight carbon nanotubes has been proposed to fabricate wearable organic thermoelectric generators.²⁵⁹ The authors demonstrated p-type and n-type films with excellent flexibility and good chemical stability at 200°C in air.

To further improve the overall performance of these implantable/wearable devices, significant efforts have focused on increasing the power density and also reducing the size of the TEGs.^{11, 256, 260-263} Developments of highly efficient TE materials and state-of-the-art manufacturing technologies have greatly advanced applications of implantable and wearable devices with miniaturized TEGs integrated as the power source.²⁶⁴⁻²⁶⁷ As shown in **Figure 13c**, a body heat-powered TEG medical device and a wireless pulse oximeter were demonstrated.²⁵² For implantable TEGs, biocompatibility and low toxicity are required for the materials or coating on the device. A biocompatible and thermally conductive membrane was applied on the surface of the device to increase the biocompatibility.²⁵⁵ In addition to implantable devices, wearable devices can also benefit from TEG as a durable power supply without recharging batteries. In order to be used in wearable devices, the flexibility of the materials and devices is

necessary. The processability of the material of choice is also critical for integration into wearable devices. To achieve this, TE materials should be printed as films or assembled as arrays on flexible substrates.¹²³ **Figure 13d** shows a flexible TE device with 72 thermoelectric modules, which lead to a power output density of 4.78 mW cm⁻² and 20.8 mW g⁻¹ in a temperature difference of 25 K.²⁵³

Conductive polymers have been widely used in biomedical devices. In recent years, tremendous work has been done to improve the conductivity of conjugated polymers and power factors for various wearable applications.²⁶⁸⁻²⁷³ The polymer nature of conductive polymers with intrinsic low κ , lightweight, good flexibility, and mechanical compliance makes them easy to be assembled, printed, or coated for TE device fabrications.^{274, 275} As discussed in the previous section, PEDOT:PSS has been intensively studied as a promising TE material.²⁷⁶ Its outstanding high σ , low κ , good thermal/chemical stability, ease of processing, and relatively high zT ²⁷⁷ make it and its composites good candidates for flexible TEGs in biomedical applications. To further improve the TE performance of such polymer TEGs, carbon nanotubes or tellurium nanowires can be incorporated.¹²³ To introduce more mechanical functionality, such as stretchability, other rubber polymers can be introduced to the conductive polymer system.²⁷⁸ By combining the discovery of the new material with modulation architecture design,^{258, 279} breakthroughs in implantable/wearable TE devices will likely be seen in the coming decades.

6.1.3 Energy harvesting from solar and nuclear sources

Solar thermoelectric generator (STEG) systems are TE devices that can supply energy from light/ solar irradiation. In general, the infrared range of the solar spectrum that provides energy for STEG is typically not useful for photovoltaics. STEGs have been studied to harvest thermal energy directly from sunlight, and these pioneering works have shown great potential in STEG as a promising sustainable alternative for energy supply.^{280, 281} For example, a flat-panel STEG with an efficiency of 4.6%, reported in Kraemer and co-workers' work, shows a decent improvement compared to past flat-panel STEGs.²⁸¹ In addition, a 3D printed concentrating STEG structure can be designed and assembled for different sun exposure conditions.²⁸² Despite these advancements, practical applications of STEGs still demand further improvement in the efficiency. Similar to photovoltaic cells, the light/energy absorption is one of the most important parameters for enhancing the power conversion efficiency, and thus the use of efficient wavelength-selective solar heat collectors and solar concentrators help further improve the device performance.¹²³ A solar concentrator in STEGs benefits from concentrating solar radiation efficiently to the devices from a large illuminated area, which leads to a high-temperature difference between the hot and cold sides of the TEG.^{283, 284} Apart from that, computer simulation and modelling is another research focus to increase the efficiency for STEGs. A modelling work reported by Baranowski et al. has shown an efficiency of 15.9% for a well-designed concentrated STEG with thermoelectric materials of $zT=1$, with a $T_h = 1000$ °C and an incident flux of 100 kW m⁻².²⁸³ With the TE materials that exhibit zT value as high as 2,

the efficiency can reach an exceedingly high value of approximately 30%.

Another advancement in STEGs is based on the combination of photovoltaic (PV) cells and TEG devices.²⁸⁵⁻²⁸⁹ Due to the radiative (also known as Shockley–Queisser limit) and non-radiative recombination of the photogenerated charge carriers, only a small portion of solar energy was transformed into electric energy. There is still a considerable amount of waste heat that can be harnessed. It has been shown that by using a spectral beam splitter,²⁹⁰ STEGs that are integrated with PV devices could remarkably increase the overall efficiency of the system, which might lead to the development of high-efficiency PV/STEG power plants. **Figure 13e** presents a printed STEG that includes 10 pairs of p-n thermoelectric legs, demonstrating an open circuit voltage of 55 mV and output power of 4.44 μ W.¹⁶¹ By applying a solar absorber on the hot end, the STEG reached a ΔT value as high as 20.9 K, overcoming the challenge of low ΔT faced by conventional wearable TEGs.

In addition to solar energy, thermoelectric devices can also harvest radioisotope energy, as used in a radioisotope thermoelectric generator (RTG).²⁹¹ RTGs use an array of thermocouples to convert the energy (heat) released by a radioactive material through its decay into electricity. Owing to several advantages including low maintenance and high energy density, general applications of RTGs include work in extreme environments, such as undersea (deep ocean) or space.^{292, 293} As an example of a long-lifespan power source,²⁹⁴ a typical RTG includes a radioisotope heat source, a radiation shielding layer, and an array of thermoelectric modules. The heat source of RTGs supplies a steady heat flow that can be converted into electricity by the TEG. Several printing techniques, such as screen printing, have been demonstrated to rapidly prototype different RTGs.^{10, 295, 296} Due to the well-controlled device geometry via printing, miniaturized radioisotope thermoelectric generators can be readily fabricated.¹⁰ With a 1.5 W isotope heat source, the printed device demonstrates an open-circuit voltage of 68.4 mV, a short-circuit current of 0.329 mA, and a maximum output power of 5.8 μ W at 39.2 mV. Despite the relatively fewer studies done on printed RTG, it is expected that the conformal and well-designed TE modules enabled by printing techniques, along with the use of the printable high- zT materials, can lead to improved efficiency and power density of RTGs for applications in extreme environments.

6.2. Temperature control and sensing

6.2.1 Thermal management and temperature control

Strategies that are based on the Seebeck effect and Peltier effect have led to device innovations in temperature sensing/control.^{123, 297-299} In fact, the Peltier effect of TE devices has been investigated extensively for thermal management and temperature control.^{300, 301} Unlike conventional fluid-based temperature control systems, TE-based temperature controllers use electrical current as the heat carrier.³⁰² A number of TE-based temperature control systems have been demonstrated including microclimate cooling systems, indoor air coolers, and wearable cooling devices.³⁰³⁻³¹¹ For example, 3D printing of nanostructured TE materials has been used to fabricate p-type Bi_{0.4}Sb_{1.6}Te₃ for TE-based cooling modules.³¹²

Owing to the high zT of printed $\text{Bi}_{0.4}\text{Sb}_{1.6}\text{Te}_3$ (maximum $zT = 1.1$), the fabricated devices demonstrated a decent cooling performance with the maximum cooling temperature difference of 62 K. As another example, Kim et al. developed a high-performance cooling device by creating a temperature difference of 81 K with $T_h = 300$ K, representing an excellent thermal management ability.¹⁷⁶ As shown in **Figure 14a**, Hong et al. reported a wearable TE device with a high coefficient of performance ($\text{COP} > 1.5$).³¹³ The authors found it can achieve >10 °C cooling effect with high flexibility, which can be attributed to the use of double elastomer layers and high- zT rigid TE pillars.³¹³ A detailed analyses of IR image showing a residual cooling effect even after removing the TE devices (**Figure 14b-c**). In addition, the authors also demonstrated the TE device mobility by combining flexible power sources to produce an all-flexible personalized temperature controller where the power coin cell batteries are embedded into an Ecoflex matrix for power supply (**Figure 14d**). By using the transient response of a current pulse, a temporary enhancement of TE cooling can be achieved.³¹⁴ Such “super-cooling” effect is able to deliver a large temperature drop temporarily and can be useful for some applications where fast cooling is important.^{315, 316} In the future, efforts will be focused on further improving the efficiency of TE devices and developing materials and fabrication techniques to reduce the cost, enabling broader applications for TE thermal management.

enable sustainable solar-driven water collection without the need for an external power supply. It was reported that a highly integrated condensation system can supply up to 1 L of freshwater per hour in a high humidity area.³²² For low-humidity regions, one possible water collection strategy is to take advantage of the moisture from plants. A prototype of a solar-driven TE water condensation system³²³ was able to harvest 10 mL of water in 3 h in the morning. Given the rapid growth of global population with high water demand, a future focus would be the highly scalable additive manufacturing techniques that provide high efficiency and low-cost TE cooling systems for water condensation.

6.2.2 Temperature sensors and other devices

Temperature sensing is based on the simple Seebeck effect of thermoelectric materials, in which an output voltage is generated by a ΔT in a circuit of two different electrical conductors.³⁰⁰ As a result, the temperature and temperature change can be monitored by measuring the generated voltage from the thermocouples. Main categories of TE-based temperature sensors include traditional metal thermocouples, bulk semiconductor thermocouples, and thin-film thermocouples. Currently, bulk semiconductors and thin-film thermocouples have been widely studied and used in several advanced fields as they are energetically efficient, vibration-free, operable under a large temperature range, and highly sensitive.³²⁴⁻³²⁹ As shown in **Figure 14e**, an array of screen-printed TE modules have been demonstrated for 3D conformal temperature detection, which can be particularly useful for temperature sensing on the surface and inside of these automotive parts.³¹⁷ Due to their reliability with minimal maintenance, thermoelectric devices can also be used for infrared radiation detection, fire alarm systems, and multi-sensing applications.³³⁰⁻³³³ In addition, thermoelectric temperature sensors are self-powered and usually dual-functional, which may enable power generation and temperature sensing simultaneously in the presence of stable heat sources.³³⁴⁻³³⁶

In comparison with conventional bulk thermocouples, micro-sized thin-film thermocouples have fast response and high sensitivity because of their low thermal mass.³³⁷ These unique properties of thin-film TE sensors make them powerful components in many emerging areas. For instance, a novel atomic force microscope can be developed using the microfabricated silicon tips and a heating element where the tip can serve as a manipulation and imaging tool for potential applications in thermomechanical writing and thermoelectric sensing.^{338, 339} Furthermore, metal oxide TE sensors have been developed with extremely high-temperature tolerance (up to 1600 K).³⁴⁰ As the performance of TE temperature sensors is highly dependent on the properties of TE materials, rational design and cutting edge fabrication techniques of high-performance TE materials can be employed to develop TE sensors with broader applications.

Based on the temperature sensing properties, various multifunctional sensing devices have been demonstrated. For example, gas sensing can be achieved by detecting heat signals

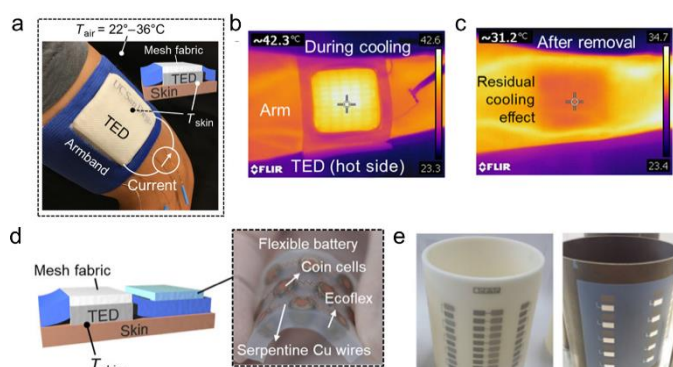


Figure 14. Examples of TE-based based thermal management and temperature control. (a) Examples of thermoregulation on human skin. (b-c) IR image of the conformal thermoelectric devices (TED, hot side) during cooling (b) as well as after removing TE devices (c). (d) An all-flexible thermoregulation device. (e) Screen-printed conformal temperature sensors on aluminum oxide (left) and steel substrates (right).³¹⁷ a-d) Adapted from ref. 313 with permission from AAAS. e) Adapted from ref. 317 with permission from AMA Science.

Another emerging application of TE cooling is fresh water harvesting directly from humid air and moist steam from unusable water via condensation.³¹⁸⁻³²¹ Based on Peltier coolers, efficient fresh water collection can be accomplished. Peltier coolers can generate a dramatic temperature drop below ambient temperature, which make it feasible to use TE materials to collect fresh water from air. In addition, solar cells can be integrated in such systems to supply power and thus can

from catalytic reactions while applying TE principles in such detection enables real-time gas sensing.³⁴¹ In 2001, Shin et al. designed a thick film NiO-based H₂ sensor, where Pt acts as a catalyst reacting with H₂ and releasing heat.³⁴¹ The generated heat creates a hot region for the TE active layer to generate voltage that can be recorded and analyzed to indicate the H₂ level. In addition to hydrogen gas, other gas detection has also been investigated, including ethanol and isopropanol vapor.³⁴² Combined with a calorimetric method, Park et al. reported a thermoelectric gas sensor that is able to not only detect CH₄, but also differentiates a mixture of CH₄ and H₂ with high resolution in the concentration range 200–2000 ppm. Pt/ α -Al₂O₃ was used as a catalyst that facilitates H₂ combustion. These thermoelectric gas sensors showed both temperature- and gas concentration-dependent responses to H₂, CH₄, and the mixed gases with a wide temperature range of 100–400 °C in air, indicating a promising low-cost alternative for gas detection with a short response time.

7. Conclusion and Future Perspectives

Printing processes offer several major advantages over conventional device fabrication methods. First of all, printing methods are highly scalable to fabricate both film-based microscale devices for small-scale energy harvesting and cooling applications and three-dimensional macroscale devices for large-scale waste heat recovery applications. Secondly, printing processes are applicable to a broad range of materials, including both organic and inorganic, and hybrid composite materials. Thirdly, printing methods are adaptable to deposit devices on 2D flexible and 3D curved substrates, enabling direct device integration onto surfaces and components for end-use applications. Future research directions that leverage advancements in nanostructured materials and emerging additive manufacturing methods should be prioritized.

To realize large-scale application and mass commercialization of printed TE materials, a comprehensive understanding and systematic optimization of thermoelectric inks, printing methods, and device applications should be meticulously considered. In the area of thermoelectric ink synthesis and formulation, tremendous research opportunities exist in designing nanoparticles with optimized surface chemistry tailored for scalable and controllable printing processes. In order to realize scalable and low-cost printing at ambient conditions, the nanoparticles need to have excellent chemical and colloidal stability to retain and translate their superior properties from nanoscale to macroscale. The ingredients (e.g., solvents, surfactants, and binders) are crucial elements in ink formulation that directly determines the quality of inks (e.g., colloidal stability and chemical stability). Therefore, innovative ink formulations that not only provide excellent processability and stability, but also are able to control and engineer energy carrier (e.g. electron and phonon) transport properties on-demand are essential for developing next-generation, high-performance TE devices. For example, composition-matched molecular binders (e.g., chalcogenidometallates) were recently developed and used to improve device performance in photovoltaics and thermoelectrics.³⁴³ Similarly, composition-matched

nanosurfactants that can greatly reduce the interfacial tension and optimize the overall functionalities of the printed devices have been developed to replace conventional surfactants in printing processes.¹⁴³ These emerging approaches could lead to the development of highly functional inks, and therefore more works need to be done on this aspect.

In the area of device design, printing and applications, even broader research opportunities emerge for developing advanced device design and printing methodologies to improve the performance and cost ratio of printed devices. The ability of the printing process to fabricate complex structures provides opportunities to innovate thermoelectric device design and achieve optimal form factors for their system applications. For example, microscale printing and device patterning of judiciously designed TE inks have been demonstrated for promising applications in energy harvesting and thermal management in integrated systems.³⁴⁴ On the other hand, the majority of printed thermoelectric materials still have inferior figure of merit compared with the best reported counterparts made by conventional methods mainly due to reduced charge carrier mobility. The printing processes often result in undesired defects (e.g., excessive porosity) which hinders charge carrier transport. In order to further improve the charge carrier transport of printed devices, methods that can control the orientation, packing, and interfaces of printed nanoparticles are highly desirable. For example, the appropriate design of sheath force in extrusion printing can promote particle alignment in the printed composite materials.³⁴⁵ Innovative post-printing processes also need to be developed in order to not only remove undesired ink additive/residues but also effectively sinter the printed particles with minimal porosity. To realize printed devices with competitive/superior performances, it is of utmost importance to establish a fundamental processing-structure-property relationship and develop closed-loop control of the printing processes. To that end, future research on advanced process monitoring and control processes, high-throughput and in-situ characterization methods, and data-driven computational techniques are needed to automatically optimize and control the printing processes to achieve desired microstructure and materials properties.

The success of realizing broad impacts of thermoelectrics relies upon a balanced and holistic investment in improving materials performance and advancing device design and manufacturing processes. While a great deal of progress has been accomplished in zT enhancement, it becomes more imperative to advance the material synthesis and device manufacturing processes in order to make thermoelectrics a competitive and commercially viable technology for a broad spectrum of waste heat recovery, energy harvesting and cooling applications. Scalable and efficient ink-based additive manufacturing technologies can significantly contribute to this endeavour, while at the same time providing fundamental insights in the processing-structure-property relationship of thermoelectric materials and systems. Owing to its highly multidisciplinary nature involving chemistry, physics, and material science, the ink-based printing processes in this review provide a versatile platform to transform a broad range of

material building blocks into functional devices, and thus will benefit a diverse set of emerging technologies, including printed electronics and sensors, energy conversion and storage systems, etc.

Conflicts of interest

There are no conflicts to declare.

Acknowledgements

Y.Z. and M.Z. acknowledge funding support from the National Science Foundation under award CMMI-1747685, and U.S. Department of Energy under awards DE-EE0009103, DE-NE0008812 and DE-NE0008701. GJS and DZ acknowledge the support of award 70NANB19H005 from U.S. Department of Commerce, National Institute of Standards and Technology as part of the Center for Hierarchical Materials Design (CHiMaD). S.L. acknowledges support from the National Science Foundation under award CMMI-1943104 and U.S. Department of Energy under awards DE-EE0009100 and DE-EE0009097.

References

1. A. I. Hochbaum, R. Chen, R. D. Delgado, W. Liang, E. C. Garnett, M. Najarian, A. Majumdar and P. Yang, *Nature*, 2008, **451**, 163-167.
2. Y. J. Kim, H. M. Gu, C. S. Kim, H. Choi, G. Lee, S. Kim, K. K. Yi, S. G. Lee and B. J. Cho, *Energy*, 2018, **162**, 526-533.
3. A. D. LaLonde, T. Ikeda and G. J. Snyder, *Review of Scientific Instruments*, 2011, **82**, 025104.
4. A. F. May, J.-P. Fleurial and G. J. Snyder, *Phys. Rev. B*, 2008, **78**, 125205.
5. H. Anno, H. Yamada, T. Nakabayashi, M. Hokazono and R. Shirataki, *Journal of Solid State Chemistry*, 2012, **193**, 94-104.
6. Y. Kawaharada, K. Kurosaki, M. Uno and S. Yamanaka, *Journal of Alloys and Compounds*, 2001, **315**, 193-197.
7. M. Zeng and Y. Zhang, *J. Mater. Chem. A*, 2019, **7**, 23301-23336.
8. C. Ou, A. L. Sangle, A. Datta, Q. Jing, T. Busolo, T. Chalklen, V. Narayan and S. Kar-Narayan, *ACS Appl. Mater. Interfaces*, 2018, **10**, 19580-19587.
9. M. R. Burton, S. Mehraban, D. Beynon, J. McGettrick, T. Watson, N. P. Lavery and M. J. Carnie, *Adv. Energy Mater.*, 2019, **9**, 1900201.
10. Z. Yuan, X. Tang, Z. Xu, J. Li, W. Chen, K. Liu, Y. Liu and Z. Zhang, *Appl. Energy*, 2018, **225**, 746-754.
11. Z. Zhang, B. Wang, J. Qiu and S. Wang, *Manufacturing Letters*, 2019, **21**, 28-34.
12. S. J. Kim, H. Choi, Y. Kim, J. H. We, J. S. Shin, H. E. Lee, M.-W. Oh, K. J. Lee and B. J. Cho, *Nano Energy*, 2017, **31**, 258-263.
13. B. Chen, M. Kruse, B. Xu, R. Tutika, W. Zheng, M. D. Bartlett, Y. Wu and J. C. Claussen, *Nanoscale*, 2019, **11**, 5222-5230.
14. J. Y. Oh, J. H. Lee, S. W. Han, S. S. Chae, E. J. Bae, Y. H. Kang, W. J. Choi, S. Y. Cho, J.-O. Lee, H. K. Baik and T. I. Lee, *Energy Environ. Sci.*, 2016, **9**, 1696-1705.
15. B. Lee, H. Cho, K. T. Park, J.-S. Kim, M. Park, H. Kim, Y. Hong and S. Chung, *Nature Communications*, 2020, **11**, 5948.
16. , !!! INVALID CITATION !!! 16, 17.
17. G. J. Snyder, in *Energy Harvesting Technologies*, eds. S. Priya and D. J. Inman, Springer US, Boston, MA, 2009, DOI: 10.1007/978-0-387-76464-1_11, pp. 325-336.
18. L. L. Baranowski, G. J. Snyder and E. S. Toberer, *Journal of Applied Physics*, 2013, **113**, 204904.
19. G. J. Snyder, J. R. Lim, C.-K. Huang and J.-P. Fleurial, *Nat. Mater.*, 2003, **2**, 528-531.
20. L. L. Baranowski, G. J. Snyder and E. S. Toberer, *Journal of Applied Physics*, 2014, **115**, 126102.
21. G. J. Snyder and E. S. Toberer, *Nat. Mater.*, 2008, **7**, 105-114.
22. F. Bonaccorso, A. Bartolotta, J. N. Coleman and C. Backes, *Adv. Mater.*, 2016, **28**, 6136-6166.
23. P. Chang, H. Mei, S. Zhou, K. G. Dassios and L. Cheng, *J. Mater. Chem. A*, 2019, **7**, 4230-4258.
24. Y. L. Kong, I. A. Tamargo, H. Kim, B. N. Johnson, M. K. Gupta, T.-W. Koh, H.-A. Chin, D. A. Steingart, B. P. Rand and M. C. McAlpine, *Nano Lett.*, 2014, **14**, 7017-7023.
25. Z. Chen, Z. Li, J. Li, C. Liu, C. Lao, Y. Fu, C. Liu, Y. Li, P. Wang and Y. He, *Journal of the European Ceramic Society*, 2019, **39**, 661-687.
26. H. Yuk, B. Lu, S. Lin, K. Qu, J. Xu, J. Luo and X. Zhao, *Nature Communications*, 2020, **11**, 1604.
27. N. C. Raut and K. Al-Shamery, *J. Mater. Chem. C*, 2018, **6**, 1618-1641.
28. A. Friederich, J. R. Binder and W. Bauer, *Journal of the American Ceramic Society*, 2013, **96**, 2093-2099.
29. G. J. Snyder, *Appl. Phys. Lett.*, 2004, **84**, 2436-2438.
30. C. L. Cramer, H. Wang and K. Ma, *Journal of Electronic Materials*, 2018, **47**, 5122-5132.
31. M. M. Mallick, L. Franke, A. G. Rösch and U. Lemmer, *ACS Energy Lett.*, 2021, **6**, 85-91.
32. X. Shi, J. Yang, J. R. Salvador, M. Chi, J. Y. Cho, H. Wang, S. Bai, J. Yang, W. Zhang and L. Chen, *J. Am. Chem. Soc.*, 2011, **133**, 7837-7846.
33. G. Tan, F. Shi, S. Hao, H. Chi, L.-D. Zhao, C. Uher, C. Wolverton, V. P. Dravid and M. G. Kanatzidis, *J. Am. Chem. Soc.*, 2015, **137**, 5100-5112.
34. B. Xu, T. Feng, Z. Li, W. Zheng and Y. Wu, *Adv. Mater.*, 2018, **30**, 1801904.
35. G. Hu, J. Kang, L. W. T. Ng, X. Zhu, R. C. T. Howe, C. G. Jones, M. C. Hersam and T. Hasan, *Chem. Soc. Rev.*, 2018, **47**, 3265-3300.
36. J. A. Lewis, *Journal of the American Ceramic Society*, 2000, **83**, 2341-2359.
37. R. J. Mehta, Y. Zhang, C. Karthik, B. Singh, R. W. Siegel, T. Borca-Tasciuc and G. Ramanath, *Nat. Mater.*, 2012, **11**, 233.
38. S. Ortega, M. Ibáñez, Y. Liu, Y. Zhang, M. V. Kovalenko, D. Cadavid and A. Cabot, *Chem. Soc. Rev.*, 2017, **46**, 3510-3528.
39. M. He, K. Kravchuk, M. Walter and M. V. Kovalenko, *Nano Lett.*, 2014, **14**, 1255-1262.
40. C. Dun, C. A. Hewitt, Q. Li, J. Xu, D. C. Schall, H. Lee, Q. Jiang and D. L. Carroll, *Adv. Mater.*, 2017, **29**, 1700070.

41. G. Zhang, B. Kirk, L. A. Jauregui, H. Yang, X. Xu, Y. P. Chen and Y. Wu, *Nano Lett.*, 2012, **12**, 56-60.
42. H. Yang, J.-H. Bahk, T. Day, A. M. S. Mohammed, B. Min, G. J. Snyder, A. Shakouri and Y. Wu, *Nano Lett.*, 2014, **14**, 5398-5404.
43. H. Yang, S. W. Finefrock, J. D. Albarracin Caballero and Y. Wu, *J. Am. Chem. Soc.*, 2014, **136**, 10242-10245.
44. M. Hong, T. C. Chasapis, Z.-G. Chen, L. Yang, M. G. Kanatzidis, G. J. Snyder and J. Zou, *ACS Nano*, 2016, **10**, 4719-4727.
45. L. Yang, Z.-G. Chen, M. Hong, L. Wang, D. Kong, L. Huang, G. Han, Y. Zou, M. Dargusch and J. Zou, *Nano Energy*, 2017, **31**, 105-112.
46. Y. Shi, L. Peng, Y. Ding, Y. Zhao and G. Yu, *Chem. Soc. Rev.*, 2015, **44**, 6684-6696.
47. T. Nezakati, A. Seifalian, A. Tan and A. M. Seifalian, *Chem. Rev.*, 2018, **118**, 6766-6843.
48. Q. Zhang, Y. Sun, W. Xu and D. Zhu, *Adv. Mater.*, 2014, **26**, 6829-6851.
49. B. Russ, A. Glauddell, J. J. Urban, M. L. Chabinyk and R. A. Segalman, *Nat. Rev. Mater.*, 2016, **1**, 16050.
50. O. Dumele, J. Chen, J. V. Passarelli and S. I. Stupp, *Adv. Mater.*, 2020, **32**, 1907247.
51. H. Yao, Z. Fan, P. Li, B. Li, X. Guan, D. Du and J. Ouyang, *J. Mater. Chem. A*, 2018, **6**, 24496-24502.
52. Y. Wang, L. Yang, X.-L. Shi, X. Shi, L. Chen, M. S. Dargusch, J. Zou and Z.-G. Chen, *Adv. Mater.*, 2019, **31**, 1807916.
53. T.-H. Le, Y. Kim and H. Yoon, *Polymers*, 2017, **9**, 150.
54. Y. Wang, Y. Shi, L. Pan, Y. Ding, Y. Zhao, Y. Li, Y. Shi and G. Yu, *Nano Lett.*, 2015, **15**, 7736-7741.
55. I. Petsagkourakis, E. Pavlopoulou, E. Cloutet, Y. F. Chen, X. Liu, M. Fahlman, M. Berggren, X. Crispin, S. Dilhaire, G. Fleury and G. Hadziioannou, *Organic Electronics*, 2018, **52**, 335-341.
56. M. Bharti, A. Singh, S. Samanta and D. K. Aswal, *Progress in Materials Science*, 2018, **93**, 270-310.
57. J. L. Bredas and G. B. Street, *Acc. Chem. Res.*, 1985, **18**, 309-315.
58. N. Lu, L. Li, N. Gao and M. Liu, *Journal of Applied Physics*, 2016, **120**, 195108.
59. D. Scheunemann and M. Kemerink, *Phys. Rev. B*, 2020, **101**, 075206.
60. X. Xu, J. Zhou and J. Chen, *Adv. Funct. Mater.*, 2020, **30**, 1904704.
61. Y. Wang, J. Zhou and R. Yang, *J. Phys. Chem. C*, 2011, **115**, 24418-24428.
62. J. Jin, Q. Wang and M. A. Haque, *Journal of Physics D: Applied Physics*, 2010, **43**, 205302.
63. S. Shen, A. Henry, J. Tong, R. Zheng and G. Chen, *Nat. Nanotechnol.*, 2010, **5**, 251-255.
64. X. Pan, A. H. P. J. Schenning, L. Shen and C. W. M. Bastiaansen, *Macromolecules*, 2020, **53**, 5599-5603.
65. S. A. Gregory, R. Hanus, A. Atassi, J. M. Rinehart, J. P. Wooding, A. K. Menon, M. D. Losego, G. J. Snyder and S. K. Yee, *Nat. Mater.*, 2021, DOI: 10.1038/s41563-021-01008-0.
66. C.-G. Han, X. Qian, Q. Li, B. Deng, Y. Zhu, Z. Han, W. Zhang, W. Wang, S.-P. Feng, G. Chen and W. Liu, *Science*, 2020, **368**, 1091-1098.
67. Y. Yang, S. W. Lee, H. Ghasemi, J. Loomis, X. Li, D. Kraemer, G. Zheng, Y. Cui and G. Chen, *PNAS*, 2014, **111**, 17011-17016.
68. J. Duan, G. Feng, B. Yu, J. Li, M. Chen, P. Yang, J. Feng, K. Liu and J. Zhou, *Nature Communications*, 2018, **9**, 5146.
69. M. A. Buckingham, K. Laws, J. T. Sengel and L. Aldous, *Green Chem.*, 2020, **22**, 6062-6074.
70. S. W. Lee, Y. Yang, H.-W. Lee, H. Ghasemi, D. Kraemer, G. Chen and Y. Cui, *Nature Communications*, 2014, **5**, 3942.
71. B. Lei, S. Bai, S. Ju, C. Yin, C. Chen and J. Zhang, *Materials Research Express*, 2021, **8**, 062001.
72. D. Zhao, A. Würger and X. Crispin, *Journal of Energy Chemistry*, 2021, **61**, 88-103.
73. J. N. Coleman, M. Lotya, A. O'Neill, S. D. Bergin, P. J. King, U. Khan, K. Young, A. Gaucher, S. De, R. J. Smith, I. V. Shvets, S. K. Arora, G. Stanton, H.-Y. Kim, K. Lee, G. T. Kim, G. S. Duesberg, T. Hallam, J. J. Boland, J. J. Wang, J. F. Donegan, J. C. Grunlan, G. Moriarty, A. Shmeliov, R. J. Nicholls, J. M. Perkins, E. M. Grievson, K. Theuwissen, D. W. McComb, P. D. Nellist and V. Nicolosi, *Science*, 2011, **331**, 568-571.
74. G. Cunningham, M. Lotya, C. S. Cucinotta, S. Sanvito, S. D. Bergin, R. Menzel, M. S. P. Shaffer and J. N. Coleman, *ACS Nano*, 2012, **6**, 3468-3480.
75. K.-G. Zhou, N.-N. Mao, H.-X. Wang, Y. Peng and H.-L. Zhang, *Angew. Chem. Int. Ed.*, 2011, **50**, 10839-10842.
76. M. Yi, Z. Shen, S. Ma and X. Zhang, *Journal of Nanoparticle Research*, 2012, **14**, 1003.
77. B. Schmatz, A. W. Lang and J. R. Reynolds, *Adv. Funct. Mater.*, 2019, DOI: 10.1002/adfm.201905266.
78. M. A. Boles, D. Ling, T. Hyeon and D. V. Talapin, *Nat. Mater.*, 2016, **15**, 141-153.
79. X. Li, Y. Qin, C. Liu, S. Jiang, L. Xiong and Q. Sun, *Food Chem.*, 2016, **199**, 356-363.
80. J. K. Lim, S. A. Majetich and R. D. Tilton, *Langmuir*, 2009, **25**, 13384-13393.
81. A. Ciesielski and P. Samori, *Chem. Soc. Rev.*, 2014, **43**, 381-398.
82. X. Wang, M. Zeng, Y.-H. Yu, H. Wang, M. S. Mannan and Z. Cheng, *ACS Appl. Mater. Interfaces*, 2017, **9**, 7852-7858.
83. M. Zeng, S. A. Shah, D. Huang, D. Parviz, Y.-H. Yu, X. Wang, M. J. Green and Z. Cheng, *ACS Appl. Mater. Interfaces*, 2017, **9**, 30797-30804.
84. J. Luo, M. Zeng, B. Peng, Y. Tang, L. Zhang, P. Wang, L. He, D. Huang, L. Wang, X. Wang, M. Chen, S. Lei, P. Lin, Y. Chen and Z. Cheng, *Angew. Chem. Int. Ed.*, 2018, **57**, 11752-11757.
85. Y.-H. Yu, Y.-P. Chen, M. Zeng and Z. Cheng, *Mater. Lett.*, 2016, **163**, 158-161.
86. P. Krishnan, A. Al-Rabbat, B. Zhang, D. Huang, L. Zhang, M. Zeng, M. S. Mannan and Z. Cheng, *Process Safety and Environmental Protection*, 2019, **123**, 48-58.
87. L. Zhang, Q. Lei, J. Luo, M. Zeng, L. Wang, D. Huang, X. Wang, S. Mannan, B. Peng and Z. Cheng, *Sci. Rep.*, 2019, **9**, 163.
88. R. Ma, M. Zeng, D. Huang, J. Wang, Z. Cheng and Q. Wang, *J. Colloid Interface Sci.*, 2021, **601**, 106-113.
89. Z. Adamczyk and P. Weroński, *Adv. Colloid Interface Sci.*, 1999, **83**, 137-226.
90. B. W. Ninham, *Adv. Colloid Interface Sci.*, 1999, **83**, 1-17.
91. S. G. Hashmi, T. Moehl, J. Halme, Y. Ma, T. Saukkonen, A. Yella, F. Giordano, J. D. Decoppet, S. M. Zakeeruddin, P. Lund and M. Grätzel, *J. Mater. Chem. A*, 2014, **2**, 19609-19615.

92. Y. Cheng, L. Zhao and T. Li, *Soft Matter*, 2014, **10**, 2714-2727.
93. T. L. Moore, L. Rodriguez-Lorenzo, V. Hirsch, S. Balog, D. Urban, C. Jud, B. Rothen-Rutishauser, M. Lattuada and A. Petri-Fink, *Chem. Soc. Rev.*, 2015, **44**, 6287-6305.
94. Z. Lin, C. Hollar, J. S. Kang, A. Yin, Y. Wang, H. Y. Shiu, Y. Huang, Y. Hu, Y. Zhang and X. Duan, *Adv. Mater.*, 2017, **29**.
95. M. V. Kovalenko, B. Spokoiny, J.-S. Lee, M. Scheele, A. Weber, S. Perera, D. Landry and D. V. Talapin, *J. Am. Chem. Soc.*, 2010, **132**, 6686-6695.
96. N. C. Anderson, M. P. Hendricks, J. J. Choi and J. S. Owen, *J. Am. Chem. Soc.*, 2013, **135**, 18536-18548.
97. A. Nag, H. Zhang, E. Janke and D. V. Talapin, *Zeitschrift für Physikalische Chemie*, 2015, **229**, 85-107.
98. T. Hasan, Z. Sun, F. Wang, F. Bonaccorso, P. H. Tan, A. G. Rozhin and A. C. Ferrari, *Adv. Mater.*, 2009, **21**, 3874-3899.
99. L. Guardia, M. J. Fernández-Merino, J. I. Paredes, P. Solís-Fernández, S. Villar-Rodil, A. Martínez-Alonso and J. M. D. Tascón, *Carbon*, 2011, **49**, 1653-1662.
100. Y. T. Liang and M. C. Hersam, *J. Am. Chem. Soc.*, 2010, **132**, 17661-17663.
101. T. Varghese, C. Dun, N. Kempf, M. Saeidi-Javash, C. Karthik, J. Richardson, C. Hollar, D. Estrada and Y. Zhang, *Adv. Funct. Mater.*, 2020, **30**, 1905796.
102. T. Varghese, C. Hollar, J. Richardson, N. Kempf, C. Han, P. Gamarachchi, D. Estrada, R. J. Mehta and Y. Zhang, *Sci. Rep.*, 2016, **6**, 33135.
103. M. Saeidi-Javash, W. Kuang, C. Dun and Y. Zhang, *Adv. Funct. Mater.*, 2019, **29**, 1901930.
104. C. Dun, W. Kuang, N. Kempf, M. Saeidi-Javash, D. J. Singh and Y. Zhang, *Adv. Sci.*, 2019, **6**, 1901788.
105. C. Ou, A. L. Sangle, T. Chalklen, Q. Jing, V. Narayan and S. Kar-Narayan, *APL Mater.*, 2018, **6**, 096101.
106. S. Ferhat, C. Domain, J. Vidal, D. Noël, B. Ratier and B. Lucas, *Sustainable Energy & Fuels*, 2018, **2**, 199-208.
107. F. Jiao, C.-a. Di, Y. Sun, P. Sheng, W. Xu and D. Zhu, *Philosophical Transactions of the Royal Society A: Mathematical, Physical and Engineering Sciences*, 2014, **372**, 20130008.
108. S. Ferhat, C. Domain, J. Vidal, D. Noël, B. Ratier and B. Lucas, *Organic Electronics*, 2019, **68**, 256-263.
109. D. Madan, Z. Wang, A. Chen, R.-c. Juang, J. Keist, P. K. Wright and J. W. Evans, *ACS Appl. Mater. Interfaces*, 2012, **4**, 6117-6124.
110. E. Jin Bae, Y. Hun Kang, K.-S. Jang and S. Yun Cho, *Sci. Rep.*, 2016, **6**, 18805.
111. F. Kim, B. Kwon, Y. Eom, J. E. Lee, S. Park, S. Jo, S. H. Park, B.-S. Kim, H. J. Im, M. H. Lee, T. S. Min, K. T. Kim, H. G. Chae, W. P. King and J. S. Son, *Nat. Energy*, 2018, **3**, 301-309.
112. C. T. Hong, Y. H. Kang, J. Ryu, S. Y. Cho and K.-S. Jang, *J. Mater. Chem. A*, 2015, **3**, 21428-21433.
113. Z. Zhang, J. Qiu and S. Wang, *Manufacturing Letters*, 2016, **8**, 6-10.
114. G. Pangalos, J. M. Dealy and M. B. Lyne, *Journal of Rheology*, 1985, **29**, 471-491.
115. X. Yang, C. Guo, L. Ji, Y. Li and Y. Tu, *Langmuir*, 2013, **29**, 8103-8107.
116. E. Küçüksönmez and J. Servantie, *Phys. Rev. E*, 2020, **102**, 012604.
117. M. Zeng, P. Wang, J. Luo, B. Peng, B. Ding, L. Zhang, L. Wang, D. Huang, I. Echols, E. Abo Deeb, E. Bordovsky, C.-H. Choi, C. Ybanez, P. Meras, E. Situ, M. S. Mannan and Z. Cheng, *ACS Appl. Mater. Interfaces*, 2018, **10**, 22793-22800.
118. A. Shinde, D. Huang, M. Saldivar, H. Xu, M. Zeng, U. Okeibunor, L. Wang, C. Mejia, P. Tin, S. George, L. Zhang and Z. Cheng, *ACS Nano*, 2019, **13**, 12461-12469.
119. M. X. Zeng, M. F. Chen, D. L. Huang, S. J. Lei, X. Zhang, L. Wang and Z. D. Cheng, *Materials Horizons*, 2021, **8**, 758-802.
120. M. Zeng, D. King, D. Huang, C. Do, L. Wang, M. Chen, S. Lei, P. Lin, Y. Chen and Z. Cheng, *PNAS*, 2019, **116**, 18322-18327.
121. J. H. We, S. J. Kim and B. J. Cho, *Energy*, 2014, **73**, 506-512.
122. Z. Lu, M. Layani, X. Zhao, L. P. Tan, T. Sun, S. Fan, Q. Yan, S. Magdassi and H. H. Hng, *Small*, 2014, **10**, 3551-3554.
123. L. Yang, Z.-G. Chen, M. S. Dargusch and J. Zou, *Adv. Energy Mater.*, 2018, **8**, 1701797.
124. M. Orrill and S. LeBlanc, *Journal of Applied Polymer Science*, 2017, **134**.
125. B. Zhang, J. Sun, H. E. Katz, F. Fang and R. L. Opila, *ACS applied materials & interfaces*, 2010, **2**, 3170-3178.
126. R. Leach, *The printing ink manual*, Springer Science & Business Media, 2012.
127. C. Xu, B. Xu, Y. Gu, Z. Xiong, J. Sun and X. S. Zhao, *Energ Environ. Sci.*, 2013, **6**, 1388-1414.
128. K. Arapov, E. Rubingh, R. Abbel, J. Laven, G. de With and H. Friedrich, *Adv. Funct. Mater.*, 2016, **26**, 586-593.
129. S. J. Kim, J. H. We and B. J. Cho, *Energ Environ. Sci.*, 2014, **7**, 1959-1965.
130. Z. Cao, M. J. Tudor, R. N. Torah and S. P. Beeby, *IEEE Transactions on Electron Devices*, 2016, **63**, 4024-4030.
131. C. Han, G. Tan, T. Varghese, M. G. Kanatzidis and Y. Zhang, *ACS Energy Lett.*, 2018, **3**, 818-822.
132. Y. Huang, H. Wu, L. Xiao, Y. Duan, H. Zhu, J. Bian, D. Ye and Z. Yin, *Materials Horizons*, 2019, **6**, 642-683.
133. B. Derby, *Annu. Rev. Mater. Res.*, 2010, **40**, 395-414.
134. J. E. Fromm, *IBM Journal of Research and Development*, 1984, **28**, 322-333.
135. F. Torrisi, T. Hasan, W. Wu, Z. Sun, A. Lombardo, T. S. Kulmala, G.-W. Hsieh, S. Jung, F. Bonaccorso, P. J. Paul, D. Chu and A. C. Ferrari, *ACS Nano*, 2012, **6**, 2992-3006.
136. D. Jang, D. Kim and J. Moon, *Langmuir*, 2009, **25**, 2629-2635.
137. T. Juntunen, H. Jussila, M. Ruoho, S. Liu, G. Hu, T. Albrow-Owen, L. W. T. Ng, R. C. T. Howe, T. Hasan, Z. Sun and I. Tittonen, *Adv. Funct. Mater.*, 2018, **28**, 1800480.
138. O. Bubnova, Z. U. Khan, A. Malti, S. Braun, M. Fahlman, M. Berggren and X. Crispin, *Nat. Mater.*, 2011, **10**, 429-433.
139. J. A. Paulsen, M. Renn, K. Christenson and R. Plourde, 2012.
140. Y. Du, R. Wang, M. Zeng, S. Xu, M. Saeidi-Javash, W. Wu and Y. Zhang, *Nano Energy*, 2021, **90**, 106522.
141. N. Turan, M. Saeidi-Javash, J. Chen, M. Zeng, Y. Zhang and D. B. Go, *ACS Appl. Mater. Interfaces*, 2021, DOI: 10.1021/acsami.1c14049.
142. M. Zeng, H. Xie, M. Saeidi-Javash, A. N. M. Tanvir, Y. Du, J. Chen, M. G. Kanatzidis and Y. Zhang, *J. Mater. Chem. A*, 2021, DOI: 10.1039/D1TA05858D.
143. M. Zeng, W. Kuang, I. Khan, D. Huang, Y. Du, M. Saeidi-Javash, L. Zhang, Z. Cheng, A. J. Hoffman and Y. Zhang, *Adv. Mater.*, 2020, **32**, e2003081.
144. D. Zhao, T. Liu, J. G. Park, M. Zhang, J.-M. Chen and B. Wang, *Microelectronic Engineering*, 2012, **96**, 71-75.

145. C. Cao, J. B. Andrews and A. D. Franklin, *Adv. Electron. Mater.*, 2017, **3**, 1700057.
146. K. Wang, Y.-H. Chang, C. Zhang and B. Wang, *Carbon*, 2016, **98**, 397-403.
147. W. Xie, X. Zhang, C. Leighton and C. D. Frisbie, *Adv. Electron. Mater.*, 2017, **3**, 1600369.
148. Y. Xiao, Master thesis, Georgia Institute of Technology, 2019.
149. M. Saeidi-Javash, Y. Du, M. Zeng, B. C. Wyatt, B. Zhang, N. Kempf, B. Anasori and Y. Zhang, *ACS Applied Electronic Materials*, 2021, **3**, 2341-2348.
150. C. Ou, L. Zhang, Q. Jing, V. Narayan and S. Kar-Narayan, *Advanced Electronic Materials*, 2020, **6**, 1900720.
151. B. Y. Ahn, E. B. Duoss, M. J. Motala, X. Guo, S.-I. Park, Y. Xiong, J. Yoon, R. G. Nuzzo, J. A. Rogers and J. A. Lewis, *Science*, 2009, **323**, 1590-1593.
152. J. J. Adams, E. B. Duoss, T. F. Malkowski, M. J. Motala, B. Y. Ahn, R. G. Nuzzo, J. T. Bernhard and J. A. Lewis, *Adv. Mater.*, 2011, **23**, 1335-1340.
153. M. A. Skylar-Scott, S. Gunasekaran and J. A. Lewis, *PNAS*, 2016, **113**, 6137-6142.
154. J. A. Lewis, J. E. Smay, J. Stuecker and J. Cesarano, *Journal of the American Ceramic Society*, 2006, **89**, 3599-3609.
155. S. V. Murphy and A. Atala, *Nat. Biotechnol.*, 2014, **32**, 773.
156. J. Peng, I. Witting, N. Geisendorfer, M. Wang, M. Chang, A. Jakus, C. Kenel, X. Yan, R. Shah, G. J. Snyder and M. Grayson, *Nature Communications*, 2019, **10**, 5590.
157. J. H. Kim, S. Lee, M. Wajahat, H. Jeong, W. S. Chang, H. J. Jeong, J.-R. Yang, J. T. Kim and S. K. Seol, *ACS Nano*, 2016, **10**, 8879-8887.
158. J. A. Lewis, *Adv. Funct. Mater.*, 2006, **16**, 2193-2204.
159. C. C. Ho, J. W. Evans and P. K. Wright, *Journal of Micromechanics and Microengineering*, 2010, **20**, 104009.
160. M. Wang, R. Gurunathan, K. Imasato, N. R. Geisendorfer, A. E. Jakus, J. Peng, R. N. Shah, M. Grayson and G. J. Snyder, *Advanced Theory and Simulations*, 2019, **2**, 1800125.
161. Y. S. Jung, D. H. Jeong, S. B. Kang, F. Kim, M. H. Jeong, K.-S. Lee, J. S. Son, J. M. Baik, J.-S. Kim and K. J. Choi, *Nano Energy*, 2017, **40**, 663-672.
162. K. T. Park, J. Choi, B. Lee, Y. Ko, K. Jo, Y. M. Lee, J. A. Lim, C. R. Park and H. Kim, *J. Mater. Chem. A*, 2018, **6**, 19727-19734.
163. D. Madan, A. Chen, P. K. Wright and J. W. Evans, *Journal of Applied Physics*, 2011, **109**, 034904.
164. D. Madan, Z. Wang, A. Chen, R. Winslow, P. K. Wright and J. W. Evans, *Appl. Phys. Lett.*, 2014, **104**, 013902.
165. A. Chen, D. Madan, P. K. Wright and J. W. Evans, *Journal of Micromechanics and Microengineering*, 2011, **21**, 104006.
166. Z. Cao, J. J. Shi, R. N. Torah, M. J. Tudor and S. P. Beeby, *Journal of Physics: Conference Series*, 2015, **660**, 012096.
167. M. Jung, J. Kim, H. Koo, W. Lee, V. Subramanian and G. Cho, *Journal of nanoscience and nanotechnology*, 2014, **14**, 1303-1317.
168. J. Hast, M. Tuomikoski, R. Suhonen, K.-L. Väisänen, M. Välimäki, T. Maaninen, P. Apilo, A. Alastalo and A. Maaninen, *SID Symposium Digest of Technical Papers*, 2013, **44**, 192-195.
169. J. Noh, D. Yeom, C. Lim, H. Cha, J. Han, J. Kim, Y. Park, V. Subramanian and G. Cho, *IEEE Transactions on Electronics Packaging Manufacturing*, 2010, **33**, 275-283.
170. E. B. Secor, S. Lim, H. Zhang, C. D. Frisbie, L. F. Francis and M. C. Hersam, *Adv. Mater.*, 2014, **26**, 4533-4538.
171. R. R. Søndergaard, M. Hösel, N. Espinosa, M. Jørgensen and F. C. Krebs, *Energy Science & Engineering*, 2013, **1**, 81-88.
172. F. Aziz and A. F. Ismail, *Materials Science in Semiconductor Processing*, 2015, **39**, 416-425.
173. E. J. Bae, Y. H. Kang, C. Lee and S. Y. Cho, *J. Mater. Chem. A*, 2017, **5**, 17867-17873.
174. S. Magdassi and A. Kamyshny, *Nanomaterials for 2D and 3D Printing*, John Wiley & Sons, 2017.
175. A. Kamyshny and S. Magdassi, *Small*, 2014, **10**, 3515-3535.
176. S. I. Kim, K. H. Lee, H. A. Mun, H. S. Kim, S. W. Hwang, J. W. Roh, D. J. Yang, W. H. Shin, X. S. Li, Y. H. Lee, G. J. Snyder and S. W. Kim, *Science*, 2015, **348**, 109-114.
177. C. Wang, W. Ping, Q. Bai, H. Cui, R. Hensleigh, R. Wang, A. H. Brozena, Z. Xu, J. Dai, Y. Pei, C. Zheng, G. Pastel, J. Gao, X. Wang, H. Wang, J.-C. Zhao, B. Yang, X. Zheng, J. Luo, Y. Mo, B. Dunn and L. Hu, *Science*, 2020, **368**, 521-526.
178. E. B. Secor, T. Z. Gao, M. H. Dos Santos, S. G. Wallace, K. W. Putz and M. C. Hersam, *ACS Appl. Mater. Interfaces*, 2017, **9**, 29418-29423.
179. A. Albrecht, A. Rivadeneyra, A. Abdellah, P. Lugli and J. F. Salmerón, *J. Mater. Chem. C*, 2016, **4**, 3546-3554.
180. R. Danaei, T. Varghese, M. Ahmadzadeh, J. McCloy, C. Hollar, M. Sadeq Saleh, J. Park, Y. Zhang and R. Panat, *Adv. Eng. Mater.*, 2019, **21**, 1800800.
181. Y. Sui, Y. Dai, C. C. Liu, R. M. Sankaran and C. A. Zorman, *Adv. Mater. Technol.*, 2019, **4**, 1900119.
182. Y. Sui, C. A. Zorman and R. M. Sankaran, *Plasma Processes and Polymers*, 2020, **17**, 2000009.
183. S. Xu, G. Zhong, C. Chen, M. Zhou, D. J. Kline, R. J. Jacob, H. Xie, S. He, Z. Huang and J. Dai, *Matter*, 2019, **1**, 759-769.
184. J. Perelaer, R. Abbel, S. Wünsch, R. Jani, T. Van Lammeren and U. S. Schubert, *Adv. Mater.*, 2012, **24**, 2620-2625.
185. J. Perelaer, M. Klokkenburg, C. E. Hendriks and U. S. Schubert, *Adv. Mater.*, 2009, **21**, 4830-4834.
186. M. Grouchko, A. Kamyshny, C. F. Mihailescu, D. F. Anghel and S. Magdassi, *ACS Nano*, 2011, **5**, 3354-3359.
187. S. Magdassi, M. Grouchko, O. Berezin and A. Kamyshny, *ACS Nano*, 2010, **4**, 1943-1948.
188. H. Ju and J. Kim, *ACS Nano*, 2016, **10**, 5730-5739.
189. H. Wang, S.-i. Yi, X. Pu and C. Yu, *ACS Appl. Mater. Interfaces*, 2015, **7**, 9589-9597.
190. L. Wang, Q. Yao, H. Bi, F. Huang, Q. Wang and L. Chen, *J. Mater. Chem. A*, 2015, **3**, 7086-7092.
191. Y. Wang, G. Liu, M. Sheng, C. Yu and Y. Deng, *J. Mater. Chem. A*, 2019, **7**, 1718-1724.
192. M. Kachanov and I. Sevostianov, *Journal of Applied Mechanics*, 2012, **79**.
193. J.-W. Jeong, W.-H. Yeo, A. Akhtar, J. J. S. Norton, Y.-J. Kwack, S. Li, S.-Y. Jung, Y. Su, W. Lee, J. Xia, H. Cheng, Y. Huang, W.-S. Choi, T. Bretl and J. A. Rogers, *Adv. Mater.*, 2013, **25**, 6839-6846.
194. D.-H. Kim, J. Viventi, J. J. Amsden, J. Xiao, L. Vigeland, Y.-S. Kim, J. A. Blanco, B. Panilaitis, E. S. Frechette, D. Contreras, D. L. Kaplan, F. G. Omenetto, Y. Huang, K.-C. Hwang, M. R. Zakin, B. Litt and J. A. Rogers, *Nat. Mater.*, 2010, **9**, 511-517.
195. J. Kim, A. Banks, H. Cheng, Z. Xie, S. Xu, K.-I. Jang, J. W. Lee, Z. Liu, P. Gutruf, X. Huang, P. Wei, F. Liu, K. Li, M. Dalal, R. Ghaffari, X. Feng, Y. Huang, S. Gupta, U. Paik and J. A. Rogers, *Small*, 2015, **11**, 906-912.
196. S. Xu, Y. Zhang, L. Jia, K. E. Mathewson, K.-I. Jang, J. Kim, H. Fu, X. Huang, P. Chava, R. Wang, S. Bhole, L. Wang, Y. J. Na,

- Y. Guan, M. Flavin, Z. Han, Y. Huang and J. A. Rogers, *Science*, 2014, **344**, 70-74.
197. X. Huang, Y. Liu, K. Chen, W.-J. Shin, C.-J. Lu, G.-W. Kong, D. Patnaik, S.-H. Lee, J. F. Cortes and J. A. Rogers, *Small*, 2014, **10**, 3083-3090.
198. D.-H. Kim, N. Lu, R. Ma, Y.-S. Kim, R.-H. Kim, S. Wang, J. Wu, S. M. Won, H. Tao, A. Islam, K. J. Yu, T.-i. Kim, R. Chowdhury, M. Ying, L. Xu, M. Li, H.-J. Chung, H. Keum, M. McCormick, P. Liu, Y.-W. Zhang, F. G. Omenetto, Y. Huang, T. Coleman and J. A. Rogers, *Science*, 2011, **333**, 838-843.
199. J.-W. Jeong, J. G. McCall, G. Shin, Y. Zhang, R. Al-Hasani, M. Kim, S. Li, J. Y. Sim, K.-I. Jang and Y. Shi, *Cell*, 2015, **162**, 662-674.
200. X. Huang, W.-H. Yeo, Y. Liu and J. A. Rogers, *Biointerphases*, 2012, **7**, 52.
201. B. Le Borgne, O. De Sagazan, S. Crand, E. Jacques and M. Harnois, *ACS Appl. Mater. Interfaces*, 2017, **9**, 29424-29429.
202. T. Ding, K. H. Chan, Y. Zhou, X.-Q. Wang, Y. Cheng, T. Li and G. W. Ho, *Nature Communications*, 2020, **11**, 6006.
203. N. Nandihalli, C.-J. Liu and T. Mori, *Nano Energy*, 2020, **78**, 105186.
204. S. Lee, S. Kim, A. Pathak, A. Tripathi, T. Qiao, Y. Lee, H. Lee and H. Y. Woo, *Macromolecular Research*, 2020, **28**, 531-552.
205. R. Dinyari, S.-B. Rim, K. Huang, P. B. Catrysse and P. Peumans, *Appl. Phys. Lett.*, 2008, **92**, 091114.
206. S.-B. Rim, P. B. Catrysse, R. Dinyari, K. Huang and P. Peumans, *Opt. Express*, 2008, **16**, 4965-4971.
207. Y. Liu, M. Pharr and G. A. Salvatore, *ACS Nano*, 2017, **11**, 9614-9635.
208. S. Wagner and S. Bauer, *MRS Bulletin*, 2012, **37**, 207-213.
209. J. Peng and G. J. Snyder, *Science*, 2019, **366**, 690-691.
210. G. A. Salvatore, N. Münzenrieder, T. Kinkeldei, L. Petti, C. Zysset, I. Strebler, L. Büthe and G. Tröster, *Nature Communications*, 2014, **5**, 2982.
211. D.-H. Kim, J.-H. Ahn, W. M. Choi, H.-S. Kim, T.-H. Kim, J. Song, Y. Y. Huang, Z. Liu, C. Lu and J. A. Rogers, *Science*, 2008, **320**, 507-511.
212. M. Kaltenbrunner, T. Sekitani, J. Reeder, T. Yokota, K. Kuribara, T. Tokuhara, M. Drack, R. Schwödiauer, I. Graz, S. Bauer-Gogonea, S. Bauer and T. Someya, *Nature*, 2013, **499**, 458-463.
213. M. Kaltenbrunner, M. S. White, E. D. Glowacki, T. Sekitani, T. Someya, N. S. Sariciftci and S. Bauer, *Nature Communications*, 2012, **3**, 770.
214. E. Artukovic, M. Kaempgen, D. S. Hecht, S. Roth and G. Grüner, *Nano Lett.*, 2005, **5**, 757-760.
215. J. Lee, T.-J. Ha, H. Li, K. N. Parrish, M. Holt, A. Dodabalapur, R. S. Ruoff and D. Akinwande, *ACS Nano*, 2013, **7**, 7744-7750.
216. Y. Wang, R. Yang, Z. Shi, L. Zhang, D. Shi, E. Wang and G. Zhang, *ACS Nano*, 2011, **5**, 3645-3650.
217. T. Sekitani, U. Zschieschang, H. Klauk and T. Someya, *Nat. Mater.*, 2010, **9**, 1015-1022.
218. C. Dagdeviren, Y. Su, P. Joe, R. Yona, Y. Liu, Y.-S. Kim, Y. Huang, A. R. Damadoran, J. Xia, L. W. Martin, Y. Huang and J. A. Rogers, *Nature Communications*, 2014, **5**, 4496.
219. T. Sekitani, S. Iba, Y. Kato, Y. Noguchi, T. Someya and T. Sakurai, *Appl. Phys. Lett.*, 2005, **87**, 173502.
220. Y. Su, S. Li, R. Li and C. Dagdeviren, *Appl. Phys. Lett.*, 2015, **107**, 041905.
221. S. Li, Y. Su and R. Li, *Proceedings of the Royal Society A: Mathematical, Physical and Engineering Sciences*, 2016, **472**, 20160087.
222. Y. Shi, C. Dagdeviren, J. A. Rogers, C. F. Gao and Y. Huang, *Journal of Applied Mechanics*, 2015, **82**.
223. W. Kim, I. Lee, D. Yoon Kim, Y.-Y. Yu, H.-Y. Jung, S. Kwon, W. Seo Park and T.-S. Kim, *Nanotechnology*, 2017, **28**, 194002.
224. T. Takahashi, K. Takei, A. G. Gillies, R. S. Fearing and A. Javey, *Nano Lett.*, 2011, **11**, 5408-5413.
225. C. F. Guo, Q. Liu, G. Wang, Y. Wang, Z. Shi, Z. Suo, C.-W. Chu and Z. Ren, *PNAS*, 2015, **112**, 12332-12337.
226. A. Miyamoto, S. Lee, N. F. Cooray, S. Lee, M. Mori, N. Matsuhisa, H. Jin, L. Yoda, T. Yokota, A. Itoh, M. Sekino, H. Kawasaki, T. Ebihara, M. Amagai and T. Someya, *Nat. Nanotechnol.*, 2017, **12**, 907-913.
227. H.-J. Kim, C. Son and B. Ziaie, *Appl. Phys. Lett.*, 2008, **92**, 011904.
228. S. Cheng, A. Rydberg, K. Hjort and Z. Wu, *Appl. Phys. Lett.*, 2009, **94**, 144103.
229. D.-Y. Khang, H. Jiang, Y. Huang and J. A. Rogers, *Science*, 2006, **311**, 208-212.
230. Y. Sun, W. M. Choi, H. Jiang, Y. Y. Huang and J. A. Rogers, *Nat. Nanotechnol.*, 2006, **1**, 201-207.
231. S.-I. Park, Y. Xiong, R.-H. Kim, P. Elvikis, M. Meitl, D.-H. Kim, J. Wu, J. Yoon, C.-J. Yu, Z. Liu, Y. Huang, K.-c. Hwang, P. Ferreira, X. Li, K. Choquette and J. A. Rogers, *Science*, 2009, **325**, 977-981.
232. D.-H. Kim, J. Song, W. M. Choi, H.-S. Kim, R.-H. Kim, Z. Liu, Y. Y. Huang, K.-C. Hwang, Y.-w. Zhang and J. A. Rogers, *PNAS*, 2008, **105**, 18675-18680.
233. Y. Ma, M. Pharr, L. Wang, J. Kim, Y. Liu, Y. Xue, R. Ning, X. Wang, H. U. Chung, X. Feng, J. A. Rogers and Y. Huang, *Small*, 2017, **13**, 1602954.
234. X. Wang, Y. Ma, Y. Xue, H. Luan, M. Pharr, X. Feng, J. A. Rogers and Y. Huang, *International Journal of Solids and Structures*, 2017, **117**, 137-142.
235. C. H. Lee, Y. Ma, K.-I. Jang, A. Banks, T. Pan, X. Feng, J. S. Kim, D. Kang, M. S. Raj, B. L. McGrane, B. Morey, X. Wang, R. Ghaffari, Y. Huang and J. A. Rogers, *Adv. Funct. Mater.*, 2015, **25**, 3698-3704.
236. Y. Yang, H. Hu, Z. Chen, Z. Wang, L. Jiang, G. Lu, X. Li, R. Chen, J. Jin, H. Kang, H. Chen, S. Lin, S. Xiao, H. Zhao, R. Xiong, J. Shi, Q. Zhou, S. Xu and Y. Chen, *Nano Lett.*, 2020, **20**, 4445-4453.
237. X. F. Zheng, C. X. Liu, Y. Y. Yan and Q. Wang, *Renewable and Sustainable Energy Reviews*, 2014, **32**, 486-503.
238. M. Zebarjadi, K. Esfarjani, M. S. Dresselhaus, Z. F. Ren and G. Chen, *Energ Environ. Sci.*, 2012, **5**, 5147-5162.
239. Q. H. Zhang, X. Y. Huang, S. Q. Bai, X. Shi, C. Uher and L. D. Chen, *Adv. Eng. Mater.*, 2016, **18**, 194-213.
240. H. Glosch, M. Ashauer, U. Pfeiffer and W. Lang, *Sensors and Actuators A: Physical*, 1999, **74**, 246-250.
241. K. Kanahashi, J. Pu and T. Takenobu, *Adv. Energy Mater.*, 2020, **n/a**, 1902842.
242. J. Yang and F. R. Stabler, *Journal of electronic materials*, 2009, **38**.
243. Y. Zhang, *ACS Energy Lett.*, 2018, **3**, 1523-1524.
244. N. Espinosa, M. Lazard, L. Aixala and H. Scherrer, *Journal of Electronic materials*, 2010, **39**, 1446-1455.
245. J. LaGrandeur, D. Crane, S. Hung, B. Mazar and A. Eder, 2006.

246. Y. Zhang, M. Cleary, X. Wang, N. Kempf, L. Schoensee, J. Yang, G. Joshi and L. Meda, *Energ. Convers. Manag.*, 2015, **105**, 946-950.
247. B. Iezzi, K. Ankireddy, J. Twiddy, M. D. Losego and J. S. Jur, *Appl. Energy*, 2017, **208**, 758-765.
248. D. Madan, Z. Wang, P. K. Wright and J. W. Evans, *Appl. Energy*, 2015, **156**, 587-592.
249. S. H. Park, S. Jo, B. Kwon, F. Kim, H. W. Ban, J. E. Lee, D. H. Gu, S. H. Lee, Y. Hwang, J.-S. Kim, D.-B. Hyun, S. Lee, K. J. Choi, W. Jo and J. S. Son, *Nature Communications*, 2016, **7**, 13403.
250. J. P. Rojas, D. Conchouso, A. Arevalo, D. Singh, I. G. Foulds and M. M. Hussain, *Nano Energy*, 2017, **31**, 296-301.
251. K. Ankireddy, B. Iezzi, M. D. Losego and J. S. Jur, presented in part at the Additive Manufacturing, Electronics and Microsystems: TechConnet Briefs, 2015.
252. V. Leonov and R. J. M. Vullers, *Journal of Renewable and Sustainable Energy*, 2009, **1**, 062701.
253. S. J. Kim, H. E. Lee, H. Choi, Y. Kim, J. H. We, J. S. Shin, K. J. Lee and B. J. Cho, *Acs Nano*, 2016, **10**, 10851-10857.
254. K. T. Settaluri, H. Lo and R. J. Ram, *Journal of Electronic Materials*, 2012, **41**, 984-988.
255. Y. Yang, X.-J. Wei and J. Liu, *Journal of Physics D: Applied Physics*, 2007, **40**, 5790.
256. V. Leonov, *IEEE Sensors Journal*, 2013, **13**, 2284-2291.
257. S. Lv, W. He, L. Wang, G. Li, J. Ji, H. Chen and G. Zhang, *Applied Thermal Engineering*, 2016, **109**, 138-146.
258. F. Suarez, A. Nozariasbmarz, D. Vashae and M. C. Öztürk, *Energ Environ. Sci.*, 2016, **9**, 2099-2113.
259. C. K. Mytafides, L. Tzounis, G. Karalis, P. Formanek and A. S. Paipetis, *ACS Appl. Mater. Interfaces*, 2021, **13**, 11151-11165.
260. J.-H. Bahk, H. Fang, K. Yazawa and A. Shakouri, *J. Mater. Chem. C*, 2015, **3**, 10362-10374.
261. M. Thielen, L. Sigrist, M. Magno, C. Hierold and L. Benini, *Energ. Convers. Manag.*, 2017, **131**, 44-54.
262. A. R. M. Siddique, S. Mahmud and B. V. Heyst, *Renewable and Sustainable Energy Reviews*, 2017, **73**, 730-744.
263. C. Hollar, Z. Lin, M. Kongara, T. Varghese, C. Karthik, J. Schimpf, J. Eixenberger, P. H. Davis, Y. Wu, X. Duan, Y. Zhang and D. Estrada, *Adv. Mater. Technol.*, 2020, **5**, 2000600.
264. M. Strasser, R. Aigner, M. Franosch and G. Wachutka, *Sensors and Actuators A: Physical*, 2002, **97**, 535-542.
265. R. Vullers, R. van Schaijk, I. Doms, C. Van Hoof and R. Mertens, *Solid-State Electronics*, 2009, **53**, 684-693.
266. M. Magno, D. Brunelli, L. Sigrist, R. Andri, L. Cavigelli, A. Gomez and L. Benini, *Sustainable Computing: Informatics and Systems*, 2016, **11**, 38-49.
267. H. G. Mond and A. Proclemer, *Pacing and clinical electrophysiology*, 2011, **34**, 1013-1027.
268. M. Eslamian, *Nano-Micro Lett.*, 2016, **9**, 3.
269. J. P. Rojas, D. Singh, D. Conchouso, A. Arevalo, I. G. Foulds and M. M. Hussain, *Nano Energy*, 2016, **30**, 691-699.
270. Z. U. Khan, J. Edberg, M. M. Hamed, R. Gabrielsson, H. Granberg, L. Wågberg, I. Engquist, M. Berggren and X. Crispin, *Adv. Mater.*, 2016, **28**, 4556-4562.
271. M. Dargusch, W.-D. Liu and Z.-G. Chen, *Adv. Sci.*, 2020, **7**, 2001362.
272. N. Wen, Z. Fan, S. Yang, Y. Zhao, T. Cong, S. Xu, H. Zhang, J. Wang, H. Huang, C. Li and L. Pan, *Nano Energy*, 2020, **78**, 105361.
273. A. Lund, Y. Tian, S. Darabi and C. Müller, *J. Power Sources*, 2020, **480**, 228836.
274. C. Yu, K. Choi, L. Yin and J. C. Grunlan, *ACS Nano*, 2011, **5**, 7885-7892.
275. T. Park, C. Park, B. Kim, H. Shin and E. Kim, *Energ Environ. Sci.*, 2013, **6**, 788-792.
276. N. Dubey and M. Leclerc, *J. Polym. Sci. Pol. Phys.*, 2011, **49**, 467-475.
277. Z. Fan, D. Du, X. Guan and J. Ouyang, *Nano Energy*, 2018, **51**, 481-488.
278. A. B. Kaiser, *Adv. Mater.*, 2001, **13**, 927-941.
279. W. Zhou, Q. Fan, Q. Zhang, L. Cai, K. Li, X. Gu, F. Yang, N. Zhang, Y. Wang and H. Liu, *Nature communications*, 2017, **8**, 1-9.
280. W. Zhu, Y. Deng, M. Gao and Y. Wang, *Energ. Convers. Manag.*, 2015, **106**, 1192-1200.
281. D. Kraemer, B. Poudel, H.-P. Feng, J. C. Caylor, B. Yu, X. Yan, Y. Ma, X. Wang, D. Wang, A. Muto, K. McEnaney, M. Chiesa, Z. Ren and G. Chen, *Nat. Mater.*, 2011, **10**, 532-538.
282. J. J. Estrada-López, A. A. Castillo-Atoche and E. Sanchez-Sinencio, *IEEE Sensors Letters*, 2019, **3**, 1-4.
283. L. L. Baranowski, G. J. Snyder and E. S. Toberer, *Energ Environ. Sci.*, 2012, **5**, 9055-9067.
284. H. Naito, Y. Kohsaka, D. Cooke and H. Arashi, *Solar Energy*, 1996, **58**, 191-195.
285. A. Shukla, K. Kant, A. Sharma and P. H. Biwole, *Sol Energ Mat Sol C*, 2017, **160**, 275-286.
286. D. Kraemer, L. Hu, A. Muto, X. Chen, G. Chen and M. Chiesa, *Appl. Phys. Lett.*, 2008, **92**, 243503.
287. W. G. J. H. M. v. Sark, *Appl. Energy*, 2011, **88**, 2785-2790.
288. Y. Vorobiev, J. González-Hernández, P. Vorobiev and L. Bulat, *Solar Energy*, 2006, **80**, 170-176.
289. E. A. Chávez-Urbiola, Y. V. Vorobiev and L. P. Bulat, *Solar Energy*, 2012, **86**, 369-378.
290. K. P. Sibin, N. Selvakumar, A. Kumar, A. Dey, N. Sridhara, H. D. Shashikala, A. K. Sharma and H. C. Barshilia, *Solar Energy*, 2017, **141**, 118-126.
291. G. H. Rinehart, *Progress in Nuclear Energy*, 2001, **39**, 305-319.
292. J. Yang and T. Caillat, *MRS Bulletin*, 2006, **31**, 224-229.
293. A. Khajepour and F. Rahmani, *Applied Radiation and Isotopes*, 2017, **119**, 51-59.
294. R. C. O'Brien, R. M. Ambrosi, N. P. Bannister, S. D. Howe and H. V. Atkinson, *Journal of Nuclear Materials*, 2008, **377**, 506-521.
295. Z. Yuan, X. Tang, Y. Liu, Z. Xu, K. Liu, J. Li, Z. Zhang and H. Wang, *J. Power Sources*, 2019, **414**, 509-516.
296. Z. Yuan, X. Tang, Y. Liu, Z. Xu, K. Liu, Z. Zhang, W. Chen and J. Li, *Sensors and Actuators A: Physical*, 2017, **267**, 496-504.
297. Z. Soleimani, S. Zoras, B. Ceranic, S. Shahzad and Y. Cui, *Sustainable Energy Technologies and Assessments*, 2020, **37**, 100604.
298. M. S. Hossain, T. Li, Y. Yu, J. Yong, J.-H. Bahk and E. Skafidas, *RSC Adv.*, 2020, **10**, 8421-8434.
299. N. Jaziri, A. Boughamouira, J. Müller, B. Mezghani, F. Tounsi and M. Ismail, *Energy Reports*, 2019, DOI: <https://doi.org/10.1016/j.egy.2019.12.011>.
300. D. M. Rowe, *Thermoelectrics handbook: macro to nano*, CRC press, 2018.
301. Y. Zhang, Y. Chen, C. Gong, J. Yang, R. Qian and Y. Wang, *Journal of Microelectromechanical Systems*, 2007, **16**, 1113-1119.

302. L. E. Bell, *Science*, 2008, **321**, 1457-1461.
303. J.-S. Ko, J.-H. Huh and J.-C. Kim, *Processes*, 2019, **7**, 98.
304. T. H. Kwan, X. Wu and Q. Yao, *Appl. Energy*, 2018, **222**, 410-422.
305. W.-H. Chen, P.-H. Wu, X.-D. Wang and Y.-L. Lin, *Energ. Convers. Manag.*, 2016, **127**, 404-415.
306. D. Guo, Q. Sheng, X. Dou, Z. Wang, L. Xie and B. Yang, *Applied Thermal Engineering*, 2020, **168**, 114888.
307. D. H. Pitaloka, R. N. Ikhsani, A. Naba and S. P. Sakti, 2019.
308. S. Kim, T. Kim, C. S. Kim, H. Choi, Y. J. Kim, G. S. Lee, O. Oh and B. J. Cho, *Soft Robotics*, 2020.
309. N. Asyiqin, M. Fadzly and T. Amarul, 2019.
310. M. H. Malakooti, N. Kazem, J. Yan, C. Pan, E. J. Markvicka, K. Matyjaszewski and C. Majidi, *Adv. Funct. Mater.*, 2019, **29**, 1906098.
311. E. W. Zaia, M. P. Gordon, P. Yuan and J. J. Urban, *Adv. Electron. Mater.*, 2019, **5**, 1800823.
312. J. Qiu, Y. Yan, T. Luo, K. Tang, L. Yao, J. Zhang, M. Zhang, X. Su, G. Tan, H. Xie, M. G. Kanatzidis, C. Uher and X. Tang, *Energ Environ. Sci.*, 2019, **12**, 3106-3117.
313. S. Hong, Y. Gu, J. K. Seo, J. Wang, P. Liu, Y. S. Meng, S. Xu and R. Chen, *Sci. Adv.*, 2019, **5**, eaaw0536.
314. G. J. Snyder, J.-P. Fleurial, T. Caillat, R. Yang and G. Chen, *Journal of Applied Physics*, 2002, **92**, 1564-1569.
315. H. Lv, X.-D. Wang, J.-H. Meng, T.-H. Wang and W.-M. Yan, *Appl. Energy*, 2016, **175**, 285-292.
316. J. B. McManus, D. D. Nelson, S. C. Herndon, J. H. Shorter, M. S. Zahniser, S. Blaser, L. Hvozdar, A. Muller, M. Giovannini and J. Faist, *Applied Physics B*, 2006, **85**, 235-241.
317. P. Gierth, L. Rebenklau, K. Augsburg, E. Bachmann and L. Niedermeyer, *Journal of Sensors and Sensor systems*, 2018, **7**, 43.
318. M. Eslami, F. Tajeddini and N. Etaati, *Energ. Convers. Manag.*, 2018, **174**, 417-429.
319. R. Peeters, H. Vanderschaeghe, J. Rongé and J. A. Martens, *Environmental Science: Water Research & Technology*, 2020, **6**, 2016-2034.
320. C. T. Hand and S. Peuker, *Heliyon*, 2019, **5**, e02752.
321. S. Lei, D. Huang, S. Liu, M. Chen, R. Ma, M. Zeng, D. Li, W. Ma, L. Wang and Z. Cheng, *J. Mater. Chem. A*, 2021, **9**, 15346-15354.
322. R. M. Atta, *International Journal of Water Resources and Arid Environments*, 2011, **1**, 142-145.
323. M. A. Muñoz-García, G. P. Moreda, M. P. Raga-Arroyo and O. Marín-González, *Computers and Electronics in Agriculture*, 2013, **93**, 60-67.
324. L. Huang, J. Chen, Z. Yu and D. Tang, *Anal. Chem.*, 2020, **92**, 2809-2814.
325. R. Feng, F. Tang, N. Zhang and X. Wang, *ACS Appl. Mater. Interfaces*, 2019, **11**, 38616-38624.
326. X. Zeng, C. Yan, L. Ren, T. Zhang, F. Zhou, X. Liang, N. Wang, R. Sun, J. B. Xu and C. P. Wong, *Adv. Electron. Mater.*, 2019, **5**, 1800612.
327. Y. Xie, T.-M. Chou, W. Yang, M. He, Y. Zhao, N. Li and Z.-H. Lin, *Semiconductor Science and Technology*, 2017, **32**, 044003.
328. M. Li, J. Chen, W. Zhong, M. Luo, W. Wang, X. Qing, Y. Lu, Q. Liu, K. Liu and Y. Wang, *ACS Sens.*, 2020, **5**, 2545-2554.
329. S. Han, F. Jiao, Z. U. Khan, J. Edberg, S. Fabiano and X. Crispin, *Advanced Functional Materials*, 2017, **27**, 1703549.
330. C.-T. Chiang and F.-W. Chang, *IEEE Sensors Journal*, 2015, **16**, 1038-1043.
331. D.-L. Wen, H.-T. Deng, X. Liu, G.-K. Li, X.-R. Zhang and X.-S. Zhang, *Microsystems & Nanoengineering*, 2020, **6**, 68.
332. L. Yang, Z.-G. Chen and J. Zou, in *Emerging Materials for Energy Conversion and Storage*, Elsevier, 2018, pp. 3-38.
333. T.-W. Shen, K.-C. Chang, C.-M. Sun and W. Fang, *Journal of Micromechanics and Microengineering*, 2019, **29**, 025007.
334. G. R. G. Nejad, F. Rahmani and G. R. Abaeiani, *Applied Radiation and Isotopes*, 2014, **86**, 46-51.
335. F. Zhang, Y. Zang, D. Huang, C.-a. Di and D. Zhu, *Nature communications*, 2015, **6**, 1-10.
336. F. Li, Y. Liu, X. Shi, H. Li, C. Wang, Q. Zhang, R. Ma and J. Liang, *Nano letters*, 2020, **20**, 6176-6184.
337. J. Zhang, P. Cheng, C. Zhang, G. Ding, L. Duan, J. Shao and Q. Wang, *The Journal of Engineering*, 2016, **2016**, 315-317.
338. U. Dürig, *Journal of Applied Physics*, 2005, **98**, 044906.
339. B. Gotsmann and U. Dürig, *Appl. Phys. Lett.*, 2005, **87**, 194102.
340. O. J. Gregory, M. Amani, I. M. Tougas and A. J. Drehman, *Journal of the American Ceramic Society*, 2012, **95**, 705-710.
341. W. Shin, K. Imai, N. Izu and N. Murayama, *Japanese Journal of Applied Physics*, 2001, **40**, L1232.
342. H. Sturm, E. Brauns, T. Seemann, V. Zoellmer and W. Lang, *Procedia Engineering*, 2010, **5**, 123-126.
343. D. S. Dolzhenkov, H. Zhang, J. Jang, J. S. Son, M. G. Panthani, T. Shibata, S. Chattopadhyay and D. V. Talapin, *Science*, 2015, **347**, 425-428.
344. F. Kim, S. E. Yang, H. Ju, S. Choo, J. Lee, G. Kim, S.-h. Jung, S. Kim, C. Cha, K. T. Kim, S. Ahn, H. G. Chae and J. S. Son, *Nat. Electron.*, 2021, **4**, 579-587.
345. Y. Qian, C. Li, Y. Qi and J. Zhong, *Carbon*, 2021, **171**, 777-784.